CRYSTALLIZATION HISTORY OF THE 1984 MAUNA LOA LAVA FLOW

Joy Crisp

Jet Propulsion Laboratory, California Institute of Technology, Pasadena,CA91109

Katharine V. Cashman

Department of Geological Sciences, University of Oregon, Eugene, OR 97403

Jennifer A. Bonini

Department of Geosciences, University of Arizona, Tucson, AZ 85721

Sarah B. Hougen

1105 Harkness Hall, 367 Cedar St., Yale University, New Haven, CT 06511

David C. Pieri

Jet Propulsion Laboratory, California Institute of Technology, Pasadena,CA91109

Abstract

During a three week eruption in 1984, Mauna Loa produced vent lavas that increased in crystal linity from <1 to 30%, and 27-km-long flows that increased in crystallinity as they moved downstream, We examined the crystallization history of these lavas using crystal-size distribution (CSD) analysis to study the rates of crystallization, viscosity increase, and latent heating. Typical average growth and nucleation rates were 5 x 10-9 cm S-l and 5 cm^{-3} S-l for microphenocrysts (20-500 μm size crystals nucleated in the rift zone) and 5 x 10-8 cm S-l and 5 x 104 cm^{-3} S-l for microlites (1-20 μm size crystals nucleated in the channel). These crystallization rates are high compared with those found in other CSD studies of igneous rocks, probably due to highly nonequilibrium conditions brought on by rapid degassing in the rift zone and cooling in the lava channel. Growth and nucleation rates decreased with time at the vent and with distance downstream. The maximum downstream total crystallinity measured is 39% (25% microlites, 14% microphenocrysts) in a quenched sample 14 km from the vent. Growth and nucleation rates cannot be calculated for postemplacement samples, but they place upper limits of 53-58% on the amount of crystallization in the channel 9-20 km from the vent. Crystallization could have been mostly responsible for the 10^5-fold downstream increase in apparent viscosity, although degassing and increasing incorporation of solid lava fragments also contributed. Another effect of crystallization on the lava flow was the sizeable latent heating (0.01 J g-' S-l over the first half of the flow length, if the crystallinity of downstream quench samples is representative of the hot fluid core), which may have been counteracted by entrainment of cooler material, Measurements of crystallization are shown to be crucial in the study of lava-flow emplacement dynamics,

Introduction

Crystallization can have a substantial impact on the heat budget and rheology of a lava flow, affecting cooling and magma viscosity during emplacement. These downstream changes are key factors controlling flow behavior and the final dimensions and morphology of a flow [e.g., *Sparks and Pinkerton, 1978; Guest et al.,* 1987], yet few measurements have been made to

document changes in crystallinity near the vent and with distance downstream. *Shaw and Swanson* [1970] inferred from a glassy groundmass that some flows of the Columbia River Basalt Group underwent almost no crystallization during flow advance. One of the other few documented examples of crystallization in a lava flow is provided by the 1947-48 Hekla flows, which were erupted extremely undercooked. The inner core of these flows did not crystallize during flow advance, but the crust, margins, and flow front were 150°C hotter downstream, due to latent heating triggered by physical mixing [*Einarsson*, 1949]. Lava flowing in tubes can maintain high temperatures [e.g., *Swanson,* 197.?; *Helz et al., 1991]* resulting in little or no increase in crystallinity downstream. For most advancing lava flows, *Marsh [1981]* asserts that crystal abundances are below 50-60%, because higher amounts will restrict flowage when bulk viscosity becomes too high. The viscosity of a dense crystal-melt suspension depends on the melt viscosity and the size distribution, shapes, orientations, and spatial distribution of the crystals [e.g.,*Cheng*, 1984; *Metzner*, 1985]. This limited assortment of evidence suggests that lava flows can experience little or up to 60% crystallization during emplacement, depending on eruption temperature, magma composition, concentration of volatiles, and physical conditions during flow.

For flows that undergo 50-60% crystallization during emplacement, the associated latent heat can have a large effect on the total heat budget of the flow. High rates of crystallization would also strongly affect bulk viscosity. We examine both of these issues in this study, each of which relate to the larger problem of understanding and predicting lava-flow behavior. Lava-flow models have been developed which are based on the assumption that the length of a flow is primarily controlled by cooling [e.g., *Pinkerton and Sparks,* 1976; *Hulme and Fielder, 1977; Guest et al., 1987; Crisp and Baloga, 1990],* but they do not consider the effects of latent heat in the core or try to quantify the associated changes in magma viscosity. Here, we attempt to use measurements of crystal content, crystal-size distributions, and flow temperatures to determine the magnitude of the effect of crystallization on the bulk viscosity and heat budget of a lava flow.

Background

This study focuses on the 1984 Mauna Loa flow, a thoroughly documented and well-sampled flow of considerable extent (27 km long). On March 25, magma rose from a storage area 3 to 4 km deep and erupted from summit vents [*Lipman and Banks*, 1987; *Lockwood et al., 1987].* Eight hours after the eruption began, the eruptive vents had moved to the 3400-3470 m elevation of the northeast rift zone, and degassing continued at the summit. After 17 hours, the magma vents migrated to their final 2800-2900 m elevation, farther down the rift zone. After March 25, degassing was restricted to the vents at 3400 m (tapping the rift zone feeder dike) and at 2800-2900 m [eruptive history provided in *Lockwood et al., 1985,* 1987; *Greenland, 1987],* Effusion rates were 4 x 10^5 to 3 x 10^6 m^3 hr^{-1} during the first two weeks and 2 x 104 to 3 x 10^5 m^3 hr^{-1} during the third and final week, releasing a total of 2.2 x 108 m^3 magma [Lipman and Banks, 1987]. Although the crystallinity was changing, the bulk composition of the tholeiitic magma was nearly constant during the eruption [*Lipman and Banks*, 1987; *Rhodes, 1988].* Field measurements taken during the eruption included temperature and velocity measurements, quench samples of magma, gas samples, measurements of levee and channel dimensions, and advance rates of the flow front *[Greenland, 1987; Lipman and Banks, 1987; Moore, 1987],*

In our study, we focus on the 1 and 1A flow lobes (Figure 1). For most of the eruption, the lava was emplaced as high-velocity (1 - 18 m S-l), open-channel aa near the vent, grading into slower (0.1 -1 m S-l) rubble-covered aa near the advancing front [*Lipman and Banks, 1987],* The 1 flow lobe began March 25, reached 25 km distance in 4 days, and attained a final length of 27 km in 5 days. The 1A flow lobe erupted from the same vents as the 1 flow lobe, but issued forth as a breakout from the 1 flow, 13 km downstream from the vents on March 29. The 1A lobe travel led most of its final length by March 31 and stopped advancing April 5. The end of advance of the 1 lobe coincides with a slight drop in effusion rate at the vent, whereas the slowdown of the 1A flow lobe occurred during a period of constant eruption rate [*Lockwood et al.,* 1985; *Lipman and Banks,* 1987]. Thus, the length of the 1 lobe may have been controlled, at least in part, by the supply rate at the vent. The 1A flow length may have been primarily controlled by cooling and crystallization

of the fluid interior.

Lipman et al. [1985] and *Lipman and Banks [1987]* identified three separate crystal populations in quenched samples: (1) phenocrysts (or xenocrysts) up to 5 mm in diameter, amounting to less than 0.5 volume% of the magma, (2) microphenocrysts, mostly ranging from 50 to 1000 μm in length, and (3) microlites less than about 10 μm across. From the timing and location of sample collection, they concluded that the phenocrysts formed at depth, the microphenocrysts nucleated and grew in the rift zone during eruption, and the microlites nucleated during flow advance after the magma left the vent.

Lipman et al. [1985] presented evidence that crystallization of the microphenocrysts was induced by degassing rather than cooling. This is consistent with the increase from less than 0.5 to 30% microphenocrysts at the vent, nearly constant vent temperatures and bulk magma chemistry, and the estimated 20-30°C undercooking [*Lipman et al.,* 1985]. This model is also supported by thermodynamic modelling [Russell, 1987], although orthopyroxene intergrown with abundant augite (Fig. *2a)* in the microphenocryst assemblage of earl y samples indicates disequilibrium conditions. If equilibrium were attained at lithostatic pressure, olivine microphenocrysts would have begun nucleating in response to degassing at pressures above the 8-15 MPa H_2O saturation level (depths of 350-650 m), and plagioclase microphenocrysts would have nucleated at depths of about 100 m *[Greenland,* 1987; *Russell, 1987].* During most of the eruption, magma travel led about 15 km through a feeder dike in the rift zone, vigorously degassing H_20 and $C0_2$ from the 3400-3470 m elevation vents, before exiting from the 2800-2900 m vents [*Greenland, 1987; Lockwood et al., 1987].* This suggests that magmatic pressures may have been less than lithostatic through much of the feeder dike system [*Spence and Turcotte,* 1985; *Lipman and Banks, 1987; Russell,* 1987]. If the feeder dike had a bladelike shape of 15 km x 3 km x 5 m, as suggested for rift dikes at Kilauea *[Dvorak et al.,* 1986; *Wilson and Head,* 1988], then the total volume of magma erupted was comparable to the volume of the dike, and degassing-induced crystallization may have occurred at shallow levels throughout most of the eruption, Microphenocrysts in the magma erupted on the last day of the eruption could have begun nucleation and growth on the first day of

the eruption; such growth would explain the increase in crystallinity at the vent as the eruption proceeded.

The large increase in microphenocryst abundance and average microphenocryst length at the vent [*Lipman and Banks*, 1987] must have strongly affected bulk rheology and dynamics of flow emplacement, The high microphenocryst abundance toward the end of the eruption limited the amount of possible microlite crystallization in the channel to 30% or less. In this study, crystal-size distributions (CSD'S) of the microphenocrysts were measured to assess the impact on rheology and to study the heat budget of the lava flow. To use our measured downstream CSD's for determining the magnitude of the latent heat and viscosity effects in the advancing lava, we have assumed that the samples are representative of the hottest portion of the fluid interior, If instead, they came from a chilled marginal zone, then the estimates of latent heat and viscosity change that we make later in this paper yield upper bounds.

Lipman and Bunks [1987] noted that the abundance of microlites increased downstream. Quantification of this increase is critical for determining the role of crystallinity in the estimated *five* orders-of-magnitude increase in apparent viscosity downstream [Mom-e, 1987]. *Lipman and Bunks [1987]* used transmitted-light microscopy to measure crystals and noted large uncertainties in counts of crystals smaller than 30 pm. We were able to measure microlites as small as $1\mu m^2$, using backscattered scanning electron microscopy (B SEM), reflected light microscopy, and transmitted-light microscopy of ultrathin sections. Our goal was to determine rates of crystallization during flow advance from quantitative measurements of crystal-size distributions. We also examined samples collected a few years after the eruption to determine whether posteruption samples can be used to assess the amount of crystallization that occurs during flow advance.

Crystal-Size-Dist.rihtion (CSD) Analysis Methods

To put constraints on thermal and theological models for the Mauna Loa lavas, crystal-size distribution analysis was used to infer rates of crystal nucleation and growth. The application of

CSD theory to the study of rocks was initiated by *Marsh* [1988] and *Cashman and Marsh [1988].* Specific CSD studies of volcanic rocks have been made of Makaopuhi lava lake [*Cashman and Marsh, 1988],* Mount St. Helens [*Cashman, 1988,* 1992], and the 1959 eruption of Kilauea [*Mangan,* 1990], Other CSD studies of igneous rocks are reviewed in *Cashman* [1990].

In this study, we used two different image processing methods to make our crystallinity measurements (Methods A and B in Appendix). Spatter samples collected near the vent contain microphenocrysts of plagioclase and pyroxene that increased in size and abundance with time (Figures *2a-b,* Table 1). Using Method A, measurements were made on five samples erupted on the first day of the eruption, when microphenocryst abundance was increasing rapidly, and eight samples collected during later stages of the eruption (Tables 1 and 2). These samples were characterized by point counts of total crystallinity and CSD measurements of the short and long axes of plagioclase microphenocrysts as viewed in BSEM photographs, as plagioclase is the most abundant microphenocryst phase. In the Mauna Loa samples, the average ratio of long to short axes is typically 6:1 for the plagioclase microphenocrysts.

A slightly different approach (Method B) was used to study plagioclase, pyroxene, and olivine microlite and microphenocryst distribution in selected vent samples, downstream samples, and postemplacement samples (Tables 1, 2, 3, and 4). Crystal areas were measured in thick sections viewed with reflected-light microscopy or in ultrathin sections (≈ 5 μm thick) viewed with transmitted-light microscopy. The size dimension used in the CSD analysis for Method B was equivalent circular diameter, L, defined as $L = 4\,(A_c/\pi)^{1/2}$, where A_c is the measured crystal area in a planar slice. This method results in a size characterization that is approximately equal to the average of long and short axis sizes. For all of the microlite measurements and some of the microphenocryst measurements, plagioclase was measured separatel y from pyroxene and olivine. It is easily distinguished from the mafic silicates by its lower reflectivity.

To analyze the crystal-size data for a sample, a frequency histogram shows the number of crystals per unit volume for different crystal-size bins (Figure 3). Ln (n) is then plotted versus crystal size (L), where $n = dN/dL$ and N is the number of crystals per unit volume less than size L

(Figure 4). Under the assumption of steady-state crystallization in a closed system with constant rates of crystal growth and nucleation, the slope of this plot is $-1/G\tau$ and the intercept at $L=0$ is $\ln(n^o)$, where no is the population density of nuclei. This allows us to solve for crystal-growth rate (G) if the duration of crystal growth (τ) is known. Nucleation rate (J) can be computed from τ and n^o, since $J = n^oG$. *Marsh [1988]* discusses the derivation and use of these equations in more detail.

For the Mauna Loa samples, crystal-size histograms (Figure 3) show an abrupt change in the number of crystals measured at a size of 20 pm, reflected as a change in slope in the CSD plot (Figure 4). This is the cutoff between what we define as microlites (< 20 μm), which nucleated and grew at the vent during lava fountaining and in the channel during emplacement, and microphenocrysts (> 20 pm), which nucleated in the rift zone before eruption onto the surface. The different degassing stages and degree of undercooking for the two crystal populations resulted in different rates of nucleation and growth, which is reflected in the slope change in the crystal-size frequency plots. This is an encouraging result for the study of other lava flows, because it shows that downstream samples can be used to separate the effects of crystallization at depth from crystallization after the lava is erupted.

Crystallization of microphenocrysts in the rift zone

Quenched samples collected at the vent show an increase in microphenocryst size and content with time (Figures *2a-b)* [*Lipman and Banks*, 1987], presumably reflecting growth at shallow depths in the rift zone in response to degassing. Crystal-size measurements for these samples are summarized in Table 1, The earliest-erupted magmas have abundant plagioclase, lesser amounts of pigeonite and augite (sometimes as rims on the pigeonite), and rare olivine. Depending on the time of collection and quench procedure, different amounts of dendritic quench crystals (primarily augite and pigeonite) formed on the rims of subhedral to euhedral microphenocrysts. In later-erupted magmas, pyroxene has roughly the same abundance as plagioclase. The average microphenocryst size is typically 40-50 /μm.

Our measurements of increasing microphenocryst content at the vent agree fairly well with those of *Lipman and Banks [1987].* The volume percent microphenocrysts at the vent increases from nearly zero to about 20% over the first 100 hours, then takes values between 15 and 25% over the next 300 hours, and between 20 and 30% over the last 100 hours (Figure 5). The early increase in volume percent microphenocrysts and fairly stable nucleation density (Figure 6) indicate an increase in average microphenocryst size during the first 100 hours. inspection of plagioclase microphenocryst size as a function of time (Figure 7) also reveals a large increase in crystal length in the first 100 hours, followed by a continued slower increase.

In Figure 5, samples taken from a perched lava pond are highlighted separately from spatter, pahoehoe, and aa to show the possible effects of different thermal histories, even near the vent. Field thermocouple measurements coincident with these samples were 1128- 1136°C [*Lipman and Banks,* 1987], significantly lower than the typical 1140"C for other types of samples. In the pond, the lava may have had more time for crystallization and cooling, resulting in a higher crystallinity than samples taken more directly from the vent. This emphasizes how rapidly conditions can change at the vent and points to the need for consistent and well-described sampling techniques.

Making the assumption that microphenocryst growth started at the onset of eruption at0100 on March 25, we calculate average growth rates of 2 x 10^{9} to 2 x 10-8 cm s^{-1} and average nucleation rates of 0.5 to 14 $cm^{-3} s^{-1}$ (Table 2). Such an assumption is consistent with the increase from no microphenocrysts at the start of the eruption to 20-30% at the end. Growth rates calculated from measurements of the long and short axes of plagioclase crystals (5 x 10^{-10} to 7 x 10-7 cm s^{-1}) bracket those for average crystal dimensions of all the microphenocryst types (plagioclase, pyroxene, and olivine) (Figure 8, Table 2), Nucleation rates based on average size measurements of microphenocrysts include data for plagioclase, pyroxene, and olivine. These average nucleation rates are roughly twice as high as those based on long and short axes of plagioclase alone (Figure 9), as suggested by the rates measured separately for different mineral types in samples NER1 2/22 and 12/27 (Table 2). The growth and nucleation rate estimates are greater than rates calculated for other volcanic systems, with the exception of rates for plagioclase microlites in the Mount St.

Helens blast dacite [*Cashman and Marsh, 1988; Mangan, 1990;* and *Cashman*, 1988, 1992]. This could be due to the extreme disequilibrium conditions for crystallization in the Mauna Loa rift zone.

All measurements show trends of growth and nucleation rates at the vent decreasing with increasing time (Figures 8, 9). Most of the change in crystallization rates occurred in the first three days. Thermocouple measurements made in the field [*Lipman and Banks,* 1987] and a geothermometer based on the CaO and MgO content of the glass, calibrated for Kilauea magma composition [*Helz and Thornber, 1987],* suggest that vent temperatures remained nearly constant through the eruption (Figure 10). Mauna Loa lavas are a slightly different composition than Kilauea lavas; thus, the glass geothermometer cannot be used to determine exact temperatures. Temperature variations indicated by variations in glass composition confirm that perched lava pond samples reached a lower temperature than vent samples, prior to quenching. The initial increase in crystallinity is probably the result of degassing rather than cooling, as concluded by *Lipman and Banks [1987]* and *Russell [1987].* In the later-erupted magmas, the plagioclase microphenocryst abundance is close to the 16% predicted by *Ghiorso*'s *[1985]* thermodynamic equilibrium model for anhydrous 1 atm conditions at 1140°C [Figure 11; *Cashman, 1990].* The decrease in crystallization rates with time at the vent probably reflects an initially large deviation from equilibrium due to depressurization in the rift zone, followed by an approach to a new equilibrium as crystallization continued [*Cashman,* 1990].

Crystallization during lava-flow emplacement

The sharp change in slope in CSD plots at about 20 μm (Figure 4) coincides with a difference between smaller homogeneous plagioclase microlites and larger zoned plagioclase that have rims similar in reflectivity and dimension (1-10 pm) to the microlites. This zonation is revealed in Nomarski reflected-light microscopy of HBF_4 -etched samples [methods described in *Wegner et al,, 1978; Wegner and Christie,* 1985], Although a similar compositional zonation pattern in the pyroxene and olivine is possible, it is not evident in Nomarski imaging of samples etched in

concentrated solutions of HBF_4, HF, and HC1 (using the etching methods of *Wegner and Christie* [1974]). During transport in the lava channel, these zoning features indicate that crystallization proceeded as a combination of growth of the previously nucleated microphenocrysts and nucleation and growth of new microlites.

To study the microphenocryst crystallization that occurred after the magma left the vent, we compare crystal-size measurements of quenched samples collected downstream with those 'near the vent (Table 3). The CSD's do not show an increase in microphenocryst abundance downstream and show a slight increase in average size of microphenocrysts downstream for only two of the samples, perhaps due to insufficient sampling and statistical uncertainty (see Appendix). This would suggest a lower growth rate for rims on the larger crystals compared to the microlites, perhaps due to differences in diffusion distances. Instead of calculating growth rates for the rims on the microphenocrysts from CSD measurements, it was easier to calculate overall average rates of crystallization for the downstream microphenocrysts, based on their final sizes, These rates for downstream samples are not significantly different than those for samples collected near the vent (downstream samples are marked with** in Table 2). For two samples, plagioclase crystals were measured separately from pyroxene, and the growth and nucleation rates calculated from their CSD's are similar for the two mineral types (samples NER1 2/22 and 12/27 in Table 2).

Most of the dramatic increase in volume percent crystals with distance travel led downstream results from nucleation and growth of microlites (Table 3). Only a few percent microlites crystallized during fountaining at the vent, as shown by microlite abundances of near-vent samples in Table 1. The microlite assemblage consists of plagioclase and clinopyroxene in subequal amounts. Thin section and preliminary microprobe investigation indicate that olivine is rare or absent in the microlite assemblage. Average microlite size is typically 5-10 μm. The duration of microlite growth (τ in Table 4) can be estimated from measurements of flow velocity in the channel [*Lipman and Banks,* 1987] and the distance the sample travelled before being quenched. Growth rates (G) obtained in this way range from 3 *x* 10-8 to 1 *x* 10-7 cm s^{-1}, and nucleation rates (J) range from 1 x 10^4 to 3 x 10^5 cm^{-3} s^{-1}, with no significant difference between the rates measured

separately for plagioclase and pyroxene (Table 4). As expected for the more extreme disequilibrium conditions, these crystallization rates for microlites are higher than those for the microphenocrysts, and the nucleation rates are higher than any previous estimates from CSD studies of other volcanic rocks [*Cashman, 1990,* 1992], This is consistent with observations [e.g., *Cashman, 1990,* 1993] that nucleation rates are more sensitive than growth rates to changes in supersaturation. Crystal growth rates of 10-5 to 10-4 cm S-l have been proposed for undercooked basaltic lavas [e.g., *Sparks and Pinkerton, 1978; Lipman et al., 1985], on* the basis of laboratory experiments of plagioclase in plagioclase-composition melt. However, these growth rates are higher than those found in natural systems because of the higher liquidus temperature, lower melt viscosity, and limited diffusion control [e.g., *Kirkpatrick, 198* 1]. Even though the Mauna Loa lava may have been significantly undercooked (20-30°C) [*Lipman et al.,* 1985; Figure 11], this study suggests that growth rates of 10-8 to 10-7 cm s^{-1} may be typical. Such growth rates correspond to those obtained in laboratory experiments of plagioclase in basaltic melt at 20-30°C undercooking, although microlite nucleation rates are 5 to 7 orders of magnitude higher than the experimental rates of *Sato et al.* [1981].

Quench samples were not collected from the second half of the flow (1 4-27 km from the vent), because of difficulty getting close to the channel zone and the limited exposure of hotter molten material (1086- 1126"C) in the distal zone of dispersed flow [*Lipman and Banks, 1987].* However, we can speculate about probable changes downstream. Assuming negligible growth of microphenoerysts during emplacement, the volume fraction ϕ of microlites expected after travel time t can be approximated as a function of growth (G) and nucleation rate (J) by the formula:

$$\phi(t) = [1 - \exp(-k_v J G^3 t^4)] (1 - \Phi_o) \quad (1)$$

where the shape factor $k_v = \bar{V} / (4 \bar{R}^3)$, $\bar{V}$ is mean crystal volume, $\bar{R}$ is mean crystal radius, and Φ_o is the volume fraction of microphenocrysts *[Kirkpatrick,* 1981; *Cashman,* 1990]. For calculations of crystallization in the Mauna Loa samples, we use the shape factor for spheres, $k_v = \pi/3$. Measured average shape factors from CSD'S range from about 0.6 to 6 for microlites and microphenocrysts; n/3 is appropriate for equant crystals and this convenient approximation does

not have a substantial impact on the results of our calculations. For sample NER1 2/27, Φ increased from about 0.14 at the vent to 0.39, 14 km downstream, in about 4 hours (Table 3). Although it took the flow front 5 days to reach 27 km from the vent, actual travel times for batches of lava in the channel were shorter. Surface flow velocities measured in the channel (average velocities in the flow roughly equal to 1/2 to 2/3 the surface velocities [Moore, 1987]) and estimates of velocities in the dispersed zone near the toe [*Lipman and Banks,* 1987] suggest that lava could have travelled most of the flow length in about 1 day. Upon reaching its terminus, the final total crystallinity Φ (Φ =$+ Φ_o) would have been less than about 0.6, according to arguments proposed by *Marsh [1981].* If G and *J* calculated for microlite growth during flow down the first 14 km of travel (in about 4 hours) remained constant throughout flow advance, the flow would have solidified well before reaching its final 27-km length. Separating equation (1) into two phases for travel over the first (subscript 1) and second (subscript 2) length of the flow gives this relation for phase 1 ($t < t_1$):

$$\phi_1(t) = [1 - \exp(-k_v J_1 G_1^3 t^4)](1 - \Phi_o) \quad (2)$$

and for phase 2 ($t_1 < t < t_2$):

$$\phi_2(t) = \phi_1(t_1) + \{1 - \exp[-k_v J_2 G_2^3 (t - t_1)^4]\}(1 - \Phi_o - \phi_1(t_1)), \quad (3)$$

which can be simplified to:

$$\phi_2(t) = \left(1 - \exp\{-k_v[J_1 G_1^3 t_1^4 + J_2 G_2^3 (t - t_1)^4]\}\right)(1 - \Phi_o) \quad (4)$$

From this, we calculate that if the growth rate stayed consistently near 5 x 10-8 cm s^{-1} during emplacement, then the average nucleation rate decreased 3 orders of magnitude from phase 1 to phase 2 (assuming 1 day for the transit time over the second half). If the microlite growth rate in phase 2 was 5 x 10"^{9} cm s^{-1} (similar to that for the microphenocrysts, and about 30 times less than for phase 1 microlites), then the average nucleation rate could have remained nearly constant over the entire flow length. The severely reduced rate of microlite crystallization over the second half of the flow (≤ 21% crystals produced in 1 day) likely resulted from an increasing approach to equilibrium. If this is true in general for lava flows, then Equation (1) should be evaluated by integrating appropriate estimates of G and *J* as smooth functions of time or at least by dividing the crystallization into two different phases as in Equations (2-4). Each phase could be represented by

its own constant G and *J*, one set for the average rates in the fast-moving channel and the other for more sluggish flow in distal zones.

Our estimates of growth and nucleation rates indicate that the microlites formed during travel in the first half of the flow length were farthest from equilibrium (peak values of G and *J*) and that near-vent microphenocrysts in the late-erupted samples and downstream microlites were closest to equilibrium (lowest *G* and *J*). This can be compared with predictions for thermodynamic equilibrium at 1 bar under anhydrous conditions (Figure 11). With near-vent temperatures consistently near 1135-1145°C, the initial batches of erupted magma would have been about 30° undercooked [*Lipman et al., 1985*], whereas later batches containing 20% microphenocrysts at the vent would have been closer to equilibrium (Figure 11). Thus, microlites formed near the vent during the first 2 days of eruption, when total crystallinity was low, must have nucleated and grown under highly nonequilibrium conditions. This is consistent with high growth and nucleation rates and rapid changes in those rates in the first 24 hours. At 14 km downstream from the vent, the lava contained about 39% crystals (sample NER 12/27) at a temperature measured in the field of about 1125*C, close to equilibrium [Figure 11; *Lipman and Banks, 1987*].

Two caveats need mention. The magma was not anhydrous, although it was low in volatiles and came close to anhydrous conditions as degassing continued [*Lipman et al., 1985; Lipman and Banks, 1987*]. The actual crystal assemblages do not compare favorably with those predicted by equilibrium (Figure 11). The percentage of olivine is much lower than that predicted for equilibrium. The orthopyroxene that crystallized when total crystallinity was still less than 15% is not predicted for equilibrium, probably because of the initial 20-30°C supercooled (non-equilibrium) state of the initial magma [*Lipman et al.*, 1985].

Crystallization after emplacement

Crystal-size distributions were obtained for five samples collected in 1987, to study the effects of slow cooling after the flow was emplaced (Tables 1, 2, and 4). These samples have 32-40% microlites and 17-24% microphenocrysts. The groundmass is not glassy; instead, the crystals

range from cryptocrystalline to < 1 μm size. Textural differences make it possible to distinguish the groundmass from microlites. The 53-58% total abundance of crystals (microphenocrysts and microlites) in these samples is within the SO-60% range believed to be the maximum possible in a moving lava flow [Marsh, 198 1; *Pinkerton and Stevenson, 1992]*. Microlite number densities ($n^oG\tau$, number of nuclei per unit volume) are in the same range (1×10^8 to 2×10^9 cm^{-3}) as for samples collected during the eruption, so most of the crystals observed in these postemplacement samples were probably created during emplacement.

In a sample collected during the eruption, 9,5 km downstream from the vent (NER 12/22, 59% total crystallinity), the crystal abundance and texture are nearly identical to that of the five postemplacement samples. The small fraction of glass in NER1 2/22 and the anhedral to subhedral fine-grained groundmass indicates continued crystallization during the sampling and air quench. In the other downstream air-quenched samples NER1 2/27 and 12/67, the groundmass is still glassy and only minor amounts of dendritic quench crystals < 1 μm in size nucleated on the larger crystals; apparently air-quenching can be sufficient to halt microlite crystallization and lock in the microlite CSD during emplacement. This conclusion emphasizes the importance of obtaining quenched samples (preferably water-quenched) if crystallization during flow emplacement is to be separated from crystallization after emplacement. If quenched samples are not obtained during an eruption, then the microlite CSD during emplacement might be preserved in spatter or uppermost flow surfaces that were quickly quenched, We have not been able to confirm this in our study,

CSD plots for the microphenocrysts and microlites in the postemplacement samples have similar slopes and intercepts as those for samples collected during emplacement (Tables 2 and 4). The duration of crystal growth (-c) is not as well constrained as for the quench samples, so growth and nucleation rates are not as precise. For the microlites in our postemplacement samples (Table 4), the CSD's indicate growth rates between 10-9 and 10^{-7} cm s^{-1} and nucleation rates between 10^3 and 105 cm^{-3} s^{-1}, if travel times in the channel were 2 to 24 hours. This is a reasonable estimate of the time required for travel 9 to 20 km from the vent, considering measured channel flow velocities [*Lipman and Banks,* 1987].

In theory, the number of microphenocrysts (or at least of the largest) per unit volume should not have changed during downstream transport. Thus, monitoring the microphenocryst number density at the vent (where sampling is easier) could potentially provide a way to estimate when a downstream sample (collected during or after the eruption) left the vent. In practice, this will work only for very early samples of the Mauna Loa flow, where number density changed rapidly. After the first few days, the change in plagioclase microphenocryst number density is not sensitive enough to be used to pinpoint the time of ejection from the vent, although there is a general trend of decreasing number density with increasing time (Figure 6).

This study serves as an example of the information that can be obtained from lava flows for which only postemplacement samples are available. Growth and nucleation rates cannot be directly calculated, because of the unknown duration of crystal growth. Changes in slope in CSD plots can be used to help distinguish crystals grown below the surface from those grown after the magma exits from a vent. In the samples of the Mauna Loa flow collected after the eruption, crystal growth during emplacement appears to have resulted in a different texture than that of postemplacement crystallization (anhedral fine-grained versus euhedral coarser-grained), although it is possible that some of the microlites may have grown after emplacement. Perhaps in other flows, comparison of quenched eruption samples with postemplacement samples will reveal more obvious differences. If crystallization conditions are sufficiently different, this could be reflected in a change in crystal morphology, mineral composition, or change in slope in a CSD plot.

Effects of crystallization and other processes on lava fiow rheology

Crystallization can play an important role in controlling the bulk rheology of a lava flow, although other potential contributions to downstream changes in bulk viscosity include loss of volatiles, addition of solid pieces of crust and levee, thickening of a solid crust, bubble shearing, and changes in melt composition as crystallization proceeds [e.g., *Lipman and Banks*, 1987; Moore, 1987]. We have tried to estimate the separate contributions of these effects to bulk viscosity changes in the Mauna Loa flow, by examining first the characteristics of near-vent lavas

as a function of time and then lavas at increasing distances from the vent, From measurements of channel geometry, topography, and flow velocity, *Moore* [1987] estimated an increase in apparent viscosity of 5 orders of magnitude from the vent to the toe of the Mauna Loa flow. Our analysis indicates that crystallization could account for much of this increase in apparent viscosity, but the complexity of the rheology of dense suspensions precludes an accurate determination of the magnitude of the effect.

Previous attempts to relate laboratory, theoretical estimates, and field observations of the rheology of lava flows have had difficulties [e.g., *Gauthier, 1973; Chester et al., 1985,* pp. 188-228]. One reason for this is that large-scale features in lava flows such as shear zones, cracks, inhomogeneous distributions of solid debris (e.g., the 1-6 m lava boats in the Mauna Loa flow [*Lipman and Banks*, 1987]), and viscosity gradients, are never reproduced in laboratory measurements and not included in the theoretical calculations. Even for the simplest situation of a basaltic melt with no bubbles or crystals, the viscosity estimated from its composition is only accurate to a factor of 2 [*Shaw*, 1972]. Despite these problems, order-of-magnitude arguments for the viscosity changes in the Mauna Loa flow can be made by analogy to experiments and theoretical relationships.

March 25-26 near-vent lava

At the beginning of the Mauna Loa eruption, melt viscosity was about 91 Pas (Table 6). The volume fraction of crystals, @, was near zero. However, the 55-65% vesicles near the vent, which gave the lava a fluffy consistency resembling whipped egg whites or cotton candy [*Lipman and Banks, 1987],* make it difficult to estimate its bulk viscosity. Froths typically have suspension viscosities that are complicated functions of shear rate and exhibit time-dependent non-Newtonian rheologic behavior [e.g., *Chester et al.,* 1985, pp. 188-228; *Bagdassarov and Dingwell, 1992; Valko′ and Economides*, 1992]. Pseudoplastic, dilatant, and viscoplastic theologies have been observed in vesicular suspensions, so the effect of bubbles on magma viscosity should be determined from comparisons made at similar shear rate [*Spera and Stein,* 1990; *Bagdassarov and*

Dingwell, 1992], Another parameter that should be similar when comparing experiments with vesicular lava flows is the dimensionless capillary number, *Cu.* The tendency for bubbles to deform by viscous flow is indicated by a *Ca* greater than about 0.1, where $Ca = \dot{\gamma}\eta_{melt}d/$ (20) , $\dot{\gamma}$ is shear rate, $\sigma \approx 0.3$ N m^{-1} is surface tension, and *d is* bubble diameter [*Murase and McBirney,* 1973; *Chester et al.,* 1985; *Spera et al., 1988;* F.J. Spera and D.J. Stein, pers. comm., 1990; *Stein and Spera,* 1992; *Bagdassarov and Dingwell,* 1993]. Unfortunate] y, there are no experimental results for bubble suspensions that even come close to matching the conditions relevant for basaltic lava flows [e.g., *Sibree,* 1934; *Sura and Panda,* 1990; *Stein and Spera,* 1992; *Bagdassarov and Dingwell,* 1992, 1993]; the closest matches are shown in Table 5.

At low shear rates, or if bubbles are small enough to remain spherical, bubbles can act like solid spheres to increase the viscosity of a gas-liquid suspension [e.g., *Taylor,* 1932; *Sibree, 1934; Shaw et al., 1968; Stein and Spera, 1992].* Effects of deformed bubbles on suspension viscosity are complicated; suspension viscosity can increase with porosity [*Stein and Spera,* 1992] or decrease [*Sura and Panda, 1990; Bagdassarov and Dingwell, 1992, 1993],* and can be dependent on shear rate [*Shaw et al., 1968].* For the Mauna Loa lava, the time scale for bubble deformation ($\tau_b = [Ca/\dot{\gamma}] \approx 0.3$ *to 7* s) [*Schowalter et al.,* 1968] is much greater than the viscous relaxation time scale of the melt ($\tau_s \approx 10^{-8}$ s) [*Dingwell and Webb, 1989],* and average shear rates are generally less than τ_b^{-1} (Table 5). *Bagdassarov and Dingwell [1993]* argue that when $\tau_b >> \tau_s$ and $\dot{\gamma} < \tau_b^{-1}$, the effect of increased vesicularity in bubble-melt suspensions is to increase bulk viscosity; when $\dot{\gamma} > \tau_b^{-1}$, increased vesicularity decreases bulk viscosity.

In the first few days of the eruption, the Mauna Loa flow was emplaced as a wide sheet advancing at about 0.014- 1,4 m s^{-1} [*Lipman and Banks,* 1987], corresponding to shear rates of about 0.005-1 s^{-1}. Unfortunately, *Moore's [1987]* estimates of apparent viscosity for the Mauna Loa flow (from channel geometry, slopes, and flow velocity) do not include any measurements near the vent at the beginning of the eruption. The effect of the bubbles, which were mostly rigid spheres early in the eruption near the vent (low *Ca* in Table 5), was probably to raise the magma viscosity above that of the melt alone (≈ 96 Pa s), since $\dot{\gamma} < \tau_b^{-1}$.

April 2 near-vent lava

Moore's earliest apparent viscosity estimate for lava near the vent is 150 Pa s for April 2 (Figure 12), when the magma contained about 15-20% crystals and 55-75% bubbles, and was quickly moving in a narrow channel [*Lipman and Banks,* 1987]. The effect of up to 25% crystals on the absolute bulk viscosity of a melt-crystal suspension is fairly well understood [e.g., *Shaw,* 1969]. The Einstein-Roscoe equation

$$\eta_{susp} = \eta_{melt} (1 - R\Phi)^{-2.5} \quad (5)$$

can be used to estimate bulk viscosity for basaltic magmas using the recommended value of $R = 1.67$ [*Marsh, 198* 1; *Pinkerton and Stevenson,* 1992]. From Equation (5) and melt viscosity estimates in Table 6, we estimate 210-300 Pa s for the crystal-melt suspension near the vent on April 2. The factor of 1.4 to 2 difference between our estimate for the crystal-melt suspension and *Moore's* [1987] field measurements is within the uncertainty of the melt viscosity [*Shaw,* 1972], indicating that the effect of bubbles on the suspension viscosity, at this time and location, may have been negligible. This is the onl y case in Table 5 where the flow rates were high enough that $\dot{\gamma} > \tau_b^{-1}$ (and this was only for the larger bubbles), which suggests that early in the eruption in the fast-moving channel zone, the effect of the bubbles may have been to lower bulk magma viscosity [*Bagdassarov and Dingwell, 1993]* perhaps accounting for the factor of 2 difference with *Moore's [1987]* estimate.

April 13 near-vent lava

At the vent, between April 2 and April 13, the apparent viscosity measured by *Moore* [1987] increased from about 1.1 x 102 to 1.1 x 10^3 Pa s (Figure 12). Porosities of quenched samples indicate high vesicularities of near-vent magma by April 13 (70-80% bubbles) [*Lipman and Banks,* 1987]. It is difficult to attribute all of the increase in apparent viscosity from April 2 and April 13 to the increase in crystallinity from about 13-20% to 21 -27% (Figure 5, Equation (5)). Instead, the increase in apparent viscosity was probably more related to the increase in bubble content and the decrease in shear rate (Table 5) associated with the decrease in eruption rate from 0.4x10^6 to 2 x

105 $m^3 h^{-1}$ over this time period [*Lipman and Banks*, 1987; Moore, 1987]. With a change from y > τ_b^{-1} toy < τ_b^{-1} at the vent from April 2 to April 13, the effect of the bubbles may have changed from decreasing bulk viscosity to increasing it [*Bagdassarov and Dingwell*, 1993].

April 6-8 lava 6-11 km downstream from vent

Crystallinity becomes more important in estimates of downstream and near-vent bulk viscosity after April 10. Using Equation (5) and melt viscosities in Table 6, we calculate 340-400 Pas for the crystal-melt suspensions of downstream samples collected April 6-8, NER12/57 (Φ = 0.22) and NER12/48 (Φ=0.24). This is only 5 to 10 times less than interpolated values from Moore's [1 987] estimates for lava on the same day, near the location where the samples NER12/57 and 12/48 were collected (vertical bars on Figure 12). This indicates that the effect of 35-50% vesicles [*Lipman and Banks*, 1987] and solid lava debris on the bulk viscosity is less than an order of magnitude.

March 30 lava 14 km downstream from vent

The Einstein-Roscoe equation (5) cannot be used on samples collected farther downstream, where crystallinities rose above 25%. Over the interval from 25 to 60% crystals, the bulk viscosity of a mafic magma can increase several orders of magnitude, but the exact relationship is not easy to predict [e.g., *Shaw, 1969; Cheng*, 1984; *Ryerson et al., 1988; Spera and Stein, 1990],* Up to a crystallinity of 40%, melt composition has a negligible effect on bulk viscosity. Its effect on a basalt is still less than an order of magnitude as crystallization increases from O to 60% (Table 6). Instead, the dramatic increase in apparent viscosity from crystallization is primarily due to increasing interactions between crystals.

Most empirical and theoretical relationships for the bulk viscosity of dense solid-liquid suspensions include the parameter Φ_m, the maximum possible packing fraction of solids, which is a complicated function of the size and shape distribution of solids, abundance of solids, shear rate, and spatial distribution of solids (e.g., alignment, clumping, nonrandom distributions) [e.g., *Wildemuth and Williams, 1984; Metzner, 1985; Kerr and Lister*, 1991]. As Φ approaches Φ_m,

suspension viscosity approaches infinity (Figure 13). Values of Φ_m can range from 0.44 for equidimensional rough crystals or smooth crystals with an aspect ratio of 6, 0.68 for monomodal smooth spheres, or greater than 0.8 for polymodal size distributions of smooth spheres [e.g., *Farris, 1968; Metzner, 1985].* Although Φ_m is affected by crystal-size distribution, some equations for the viscosity of solid-liquid suspensions also include separate terms for the mean and standard deviation of particle diameter [e.g., *Gay et al.,* 1969; *McBirney and Murase, 1984].* However, the relationship of *McBirney and Murase [1984]* and *Murase et al. [1985] is* not recommended for application to crystal-suspension magmas [*Pinkerton and Stevenson,* 1992],

In the Mauna Loa flow, as the rate of shear and crystal-size distribution changed during flow advance, Φ_m would have also changed with time and distance from the vent, The effect of an increasing y microlite-rich crystal-size distribution would have been to increase Φ_m, but the effect of decreasing shear rate would have been to decrease Φ_m [*Wildemuth and Williams,* 1984]. The crystallinity of sample NER1 2/27 in the rapid] y flowing channel and Shaw's measurements of apparent viscosity (Figure 12) indicate that Φ_m was greater than 0.4 on March 30, 14 km from the vent. Although the cooling history of a lava lake results in a different crystal-size distribution than for a lava flow, drilling studies of Hawaiian lava lakes found a sharp increase in rigidity at 1065-1070°C, suggesting a Φ_m of approximately 0.5 [Wright *and Okamura, 1977; Peck, 1978; Wright and Peck, 1978].* Another indication of an appropriate estimate for Φ_m is given by the arguments made by *Marsh [1981],* which suggest Φ_m is 0.5-0,6 for most lava flows. For Φ_m between 0.44 and 0.6, Table 7 shows the crystal-melt viscosity for sample NER 12/27 (Φ = 0.39, 14 km downstream from vent), as predicted by various theoretical and empirical relationships. The bulk viscosity estimates for Φ_m = 0,44 (Table 7) are close to *Moore's [1987]* estimates of apparent viscosity. However, the texture of 39% crystallinity as seen in thin section is far from closely packed, suggesting Φ_m >>0.4, since Φ_m (the maximum attainable packing fraction of solids) will increase as the CSD becomes more microlite-rich. Also, the crystallinity of postemplacement samples (microlites and microphenocrysts, but not including groundmass) suggest a Φ_m of 20.58. The minimum and maximum values in Table 7 for Φ_m = 0,5-0.6 (η_{susp} = 860-5200 Pas) are plotted as

points on Figure 12 (March 30), and are 2 to 23 times lower than Moore's [1987] estimates, although his measurements also include the apparent viscosity-increasing effects of bubbles (FY 25% vesicularity, $Ca \approx 0,3\text{-}8$), and chunks of levee and crust which are more abundant at this far downstream location compared to locations near the vent.

April 2-3.26 km downstream from vent

We do not have any samples collected during the eruption near the flow front, where *Moore* [1987] estimated an apparent viscosity of 107 Pas, *Lipman and Banks [1987]* did not measure the density of flow-front samples collected April 2-3, but their other downstream measurements suggest a porosity of a few percent or less, with minimal influence of bubbles on bulk viscosity (because of the low volume fraction). At low flow velocities over the distal half of the flow, there were several days available for continued crystal nucleation and growth beyond the 39% crystallinity found in NER1 2/27 (14 km from the vent, March 30). As the abundance of microlites increased, Φ_m may have also increased, due to ease in packing smaller crystals between the microphenocrysts. Moore's estimate of 107 Pas is consistent with $\Phi \approx 0.995\ \Phi_m$, for Φ_m between 0,4-0.6. The downstream increase in thicker crust and solid lava chunks would have also contributed to a high bulk viscosity at the toe of the flow [Moore, 1987; *Stasiuk et al.,* 1993], which suggests Φ_m was closer to 0.6.

Figure 13 demonstrates theoretical predictions for the crystal-melt suspension as a function of crystallinity and Φ_m, taking into account the changing melt viscosity. Although theoretical models cannot be used to calculate the precise bulk viscosity at the end of the Mauna Loa flow, Figure 13 shows that an increase of several orders of magnitude over the viscosity of the melt phase is clearly possible, as crystallinity approaches maximum packing levels.

Comparison with other examples of viscosity changes in lava flows

A few other examples of downstream viscosity increase in lava flows can be found in the literature. An estimated increase of apparent viscosity for a blocky andesite flow of 4 orders of

magnitude over 264 days occurred during the eruption of Lonquimay [*Naranjo et al.,* 1992]. However, the increase for Lonquimay was only 2 orders of magnitude over the same time interval it took the Mauna Loa flow to increase 105 times [Moore, 1987]. 1983-4 Puu Oo flows experienced downstream increases in apparent viscosity of 2 or 3 orders of magnitude during emplacement periods of 2-5 days [*Baloga and Crisp, 1988; Fink and Zimbelman, 1990],* and the apparent viscosity of the 1977 Puu Kiai flows is estimated to have increased 2 orders of magnitude downstream [Moore *and Ackerman, 1989].* Estimates for the 1971 lavas from Mount Etna indicate apparent viscosities of about 10^3 Pas at the vent, 10s Pas 4 km from the vent, and 107 Pas 8 km from the vent [*Booth and Self,* 1973], These increases are not as large as the five-orders-of-magnitude increase suggested for the Mauna Loa flow, perhaps because of the higher initial crystal content at the Etna vent and lower rates of crystallization in the Puu Oo flows. The estimate of a final apparent viscosity of 10^7 Pa s for both the Mauna Loa and Etna flows suggests that these flows reached a similar state of crystal "clogging" in their final stages of advance.

Yield strength

Measurements of channel morphology, slope, and velocities of the Mauna Loa flow indicate that the lava may have been Newtonian near the vent (zero yield strength), becoming Bingham ($\tau_y \approx$ 1()-100 Pa) and then pseudoplastic ($\tau_y \geq$ 2000 Pa) as it flowed downstream [Moore, 1987]. We did not attempt to estimate the yield strength of the near-vent frothy lava, due to a lack of directly applicable experiments and tested theoretical equations. For a few of the downstream samples, Table 8 shows the results of using three different approaches to try to infer yield strength of the crystal-melt suspensions from the total crystallinity and crystal-size distribution. Moore's [1987] estimates of yield strength for the downstream lava include the additional effects of bubbles, crust, and solid lava blocks. The method of *Gay et al. [1969]* predicts extremely low yield strengths (Table 8), based on experiments of particle suspensions having log-normal size distributions. Although this equation was used on lavas by *Pinkerton and Stevenson* [1992], it is not recommended here because the results are sensitive to the geometric mean and standard deviation,

and crystal-size distributions in the Mauna Loa samples are not log-normal.

Barnes and Walters [1985] and *Kerr and Lister [1991]* have warned that yield strengths extrapolated from laboratory data can simply be artifacts, which would be readjusted to lower values if theological measurements were made at lower shear rates, As long as laboratory yield strengths are measured at shear rates similar to those in the lava flow, they can be treated as apparent yield strengths and used in comparisons [F.J. Spera and D.J. Stein, unpublished report presented at the MEVTV workshop on the Evolution of Magma bodies on Mars, San Diego, CA, Jan 15-17, 1990]. Shear rates in the Mauna Loa flow for the samples in Table 8 were approximately 0.2-0.6 s^{-1} (Table 5), favoring use of the low-shear rate equation of Spera and Stein for estimating yield strength.

Effect of crystallization on heat budget

Assuming that the downstream samples represent the hottest portions of the interior flow, then over the first half of the flow length about 25% microlite crystallization released about 0.01 J s^{-1} of latent heat per gram of lava. Over the second half of the flow length, up to an additional 5-35% microlites were produced over about a day, corresponding to a latent heat of 0,0002-0,001 J g^{-1} s^{-1}. The rate of heating is at least an order of magnitude lower in these later stages, but the total number of Joules released is significant because of the lower flow velocity.

Some theoretical models for lava-flow emplacement have considered only latent heat in the crust of a lava flow, which is conducted away toward the flow surface [e.g., *Head and Wilson,* 1986]. However, the high rates of growth and nucleation of microlites estimated for downstream quench dip samples of the Mauna Loa flow indicate that latent heating within the core of a flow could also be important, To demonstrate the potential importance of latent heat to the thermal history of a flow, we make an assessment of the heat budget of the core of the Mauna Loa flow, assuming that the crystallinity of the downstream samples represents that of the hottest interior fluid portions. Figure 11 shows that the first 30% crystals could have formed in response to degassing alone, and does not require cooling in a chilled margin. The three downstream samples

(NER12/27, 12/48, and 12/57, at 6 to 14 km from the vent) were collected from brightly incandescent parts of mobile aa overflows that had spilled over the main aa channel. Samples NER1 2/27 and 12/57 did not have coincident thermocouple measurements, but 1133°C was obtained for NER12/48, which is just 7°C below temperatures at the vent [*Lipman and Banks,* 1987]. Although the flow was not in a turbulent state, the fluid interior over the first half of the flow length was probably well mixed (not simple Couette flow with parallel streamlines) as a result of changes in slope and channel width, basal topography, surges (up to 2-3 m change in 5 minutes), standing waves (exposing incandescent lava), and large blocks of eroded levee that disrupted flow streamlines [*Lipman and Banks, 1987]. Lipman and Banks [1987,* p. 1567] noted that "intricate eddies and even reverse flow, analogous to any high-energy water stream, were also common," Occasionally, vigorous surges in the channel overspilled the levees, sending aa pouring down the rubbly slopes of the levee, exposing much incandescent material in the process [*Lipman and Banks,* 1987; Moore, 1987], which would have promoted agitation and stirring. Although we have no direct evidence for the degree of mixing inside the flow, we will assume that the downstream samples are representative of the hottest portions of lava in the main channel.

With typically 15-20% microphenocrysts at the vent, rapid microlite crystallization in the channel (13-25% in 1-4 hours, Tables 3 and 4), and an upper limit of about 60% for the maximum crystallinity in the flowing lava, we estimate an average of about 25 to 45% crystallization in the channel during emplacement, The associated latent heat, expressed in Joules per gram of lava in the fluid core, is shown in Table 9. In addition to latent heat, we also estimated the effects of viscous heating and radiative and convective losses [*Crisp and Baloga, 1990]* on the total heat budget of the core. Considering just these four processes, the prediction is a sizeable net downstream heating (Table 9), which does not agree with the increasing crystallinity or the measured decrease in downstream core temperature [*Lipman and Banks,* 1987]. The discrepancy is worse over the first 12 hours of the eruption, when crystallization rates were highest (Table 9). If the downstream samples are truly representative of the crystallization of the hottest interior of the flow, then an additional cooling mechanism not shown in Table 9 must have been effective in

counteracting the latent heat. Conduction to the ground and to the upper crust during flow emplacement would affect only the cooling of the thermal boundary layers and reduce core thickness. Cooling during lava-flow advance resulting from the vaporization and expansion of volatiles would have been minimal [*Boyd*, 1961], since only a few tenths of a weight percent volatiles were present in the lava channel [*Lipman et al.*, 1985; *Lipman and Banks*, 1987]. The most likely cooling mechanism that could significant y lower core temperature is mixing and entrainment of cooler material into the core, as suggested by the abundant incandescent clots, blocks of levee, and semisolid pieces seen falling or pulled into the fluid portions of the flow (at least over the first half of the flow length). The evidence of thermal erosion or remelting of crust is indirect. Channel bottoms close to preeruption topography suggest that the initially deposited lower rubble zones were caught up into the flow. Also, the debris caught up in the flow spanned a broad spectrum of sizes and temperatures, with the smallest and hottest being extremely susceptible to reincorporation by partial melting [*Lipman and Banks*, 1987; *Moore*, *1987]*. A new thermal model that incorporates latent heating and entrainment of crust has been applied to the Mauna Loa 1984 lava and estimates of entrainment rates are given in those studies *[Crisp and Baloga*, 1992; 1993].

Sparks and Pinkerton [1978] argue that degassing should be more effective than atmospheric cooling for promoting crystallization and changing rheology, but both mechanisms, in addition to entrainment of cooler crust into the core, were important in the Mauna Loa flow. The steepness of the crystallization-temperature plot (Figure 11) in the 1120-1140°C region indicates that crystallinity would have been highly sensitive to slight changes in temperature. Figure 11 indicates that undercooking from degassing may have been responsible for about 27% of the crystals initially formed. Thereafter, a drop in temperature of about 14°C over the first half of the flow may have contributed to about a 12% increase in crystallinity, followed by another roughly 14°C cooling and 21% increase in crystallinity over the second half of the flow length (if final crystallinity reached 60%).

Summary of Important Results

The rate of microphenocryst crystallization in the Mauna Loa rift zone decreased as the magma approached equilibrium and the rate of lava production decreased, During transport in the channel, the lava was far from equilibrium and subject to high rates of crystal growth and nucleation. The rate of microlite crystallization was lower during the last half of the flow length compared to the first half, and this may be a common occurrence in other lava flows as a new equilibrium is approached after degassing.

Rift-zone crystallization can be distinguished from posteruption crystallization by the change of slope on a CSD plot. We cannot estimate exact growth and nucleation rates for crystals in samples collected after the eruption but can place a maximum bound on the amount of crystallization in the channel. Our study has shown that quenched samples collected downstream from the vent are essential for documenting the crystallization during lava-flow emplacement and are easier to interpret than samples collected after an eruption.

The bulk viscosity and rate of advance of the Mauna Loa flow were strongly affected by increasing crystallinity downstream, but we cannot estimate the precise magnitude of the rheologic changes, because of the complexity of dense suspension rheology. However, crystallization could account for most of the 107-fold increase in apparent viscosity [*Moore*, 1987].

Models for basaltic lava flows can now incorporate estimates of growth (G) and nucleation rates (*J*) for degassing-induced crystallization of microlites (G ≈ 10-7 cm s^{-1} and *J* ≈ 10s cm^{-3} s^{-1}, for fast-moving channel flow, perhaps G ≈ 10-8 cm S-l and *J* ≈ 5 x 10^3 cm^{-3} s^{-1} for slow-moving distal zones). With these rapid rates of crystallization, a tremendous amount of latent heat can be released during the emplacement of a lava flow, and this should be included in lava-flow models. In the Mauna Loa flow, this latent heat may have been counteracted by entrainment of cooler material from the levees, base, and crust [*Crisp and Baloga*, 1993].

Acknowledgments

We thank J. Lockwood of the U.S Geological Survey at the Hawaiian Volcano Observatory for generously providing us with samples of the 1984 lavas that were collected during the eruption by N. Banks, D. Clague, T. Duggan, J. Eaby, M. Garcia, P. Lipman, R. Moore, T. Neal, M. Rhodes, S. Rowland, J. Sinton, and E. Wolfe. We are grateful to M. Ghiorso for providing calculations of equilibrium crystal assemblages using his SILMIN computer model. Some of this study was conducted by J.A. Bonini and S.B. Hougen as part of their Junior Independent Work Requirements, while they were undergraduate geology majors at Princeton University, Useful comments were provided by reviews from S. Finnemore, M. Stasiuk, D. Swanson, and J. Zimbelman. Assistance with rheology and heat budget calculations was provided by S. Baloga, F. Spera, and H. Pinkerton. K. V. Cashman acknowledges support for this work from NSF award EAR 8916930. The work by J. Crisp was carried out at the Jet Propulsion Laboratory, California Institute of Technology, under a contract with the National Aeronautics and Space Administration,

References

Baloga, S., and J. Crisp, Simulations of lava flows on Mars (abstract), in *MEVTV Working Group Meeting on the volcanic evolution of Mars, LPI Contribution No. 660,* pp. 27-29, Lunar and Planetary Institute, Houston, 1988.

Bagdassarov, N.Sh., and D.B. Dingwell, A theological investigation of vesicular rhyolite, *J. Volcanol. Geotherm. Res., 40,307-322, 1992.*

Bagdassarov, N. S., and D.B. Dingwell, Frequency dependent rheology of vesicular rhyolite, *J. Geophys. Res.,* 98,6477-6487, 1993.

Barnes, H. A., and K. Walters, The yield stress myth?, *Rheol. Acts, 24,323-326, 1985.*

Booth, B., and S. Self, Theological features of the 1971 Mount Etna lavas, *Phil. Trans. R. Sot. London, Ser. A, 274,99-106, 1973.*

Boyd, F.R., Welded tuffs and flows in the rhyolite plateau of Yellowstone Park, Wyoming, *Geol. Sot. Am.* Bull., 72,387-426, 1961.

Carslaw, H. S., and J.C. Jaeger, *Conduction of heat in solids,* 2nd edition, 510 pp., Oxford Univ. Press, Oxford, 1959.

Cashman, K.V., Crystallization of Mount St. Helens 1980-1986 dacite: a quantitative approach, *Contrib. Mineral. Petrol., SO,* 194-209, 1988.

Cashman, K, V., Textural constraints on the kinetics of crystallization of igneous rocks, in *Modern methods of igneous petrology: Understanding magmatic processes,* edited by J. Nicholls and J.K. Russell, *Reviews in Mineral., 24,259-314, 1990.*

Cashman, K.V., Groundmass crystallization of Mount St, Helens dacite, 1980-1986: a tool for interpreting shallow magmatic processes, *Contrib. Mineral. Petrol., 109, 431-449, 1992.*

Cashman, K. V., Relationship between plagioclase crystallization and cooling rate in basaltic melts, *Contrib. Mineral. Petrol., 113, 126-142, 1993.*

Cashman, K.V., and B.D. Marsh, Crystal size distribution (CSD) in rocks and the kinetics and dynamics of crystallization, 11: Makaopuhi lava lake, *Contrib. Mineral. Petrol., 99,292-305, 1988.*

Cashman, K. V., M.T. Mangan, and S, Newman, Surface modification of vesicle size distributions in Kilauea basalt-Implications for interpretation of vesicle distributions in lava flows (abstract), *EOS Trans. AGU, 73,629,1992.*

Cheng, D, C.-H., Further observations on the theological behaviour of dense suspensions, *Powder Technol., 37,255-273, 1984.*

Chester, D.K., A.M. Duncan, J.E. Guest, and C.R.J. Kilburn, *Mount Etna: The anatomy of a volcano, 404* pp., Stanford Univ. Press, Stanford, CA, 1985.

Crisp, J., and S. Baloga, A model for lava flows with two thermal components, *J. Geophys. Res.,* 9.5, 1255-1270, 1990.

Crisp, J., and S. Baloga, The influence of crystallization and entrainment on the emplacement of lava flows (abstract), *23rd Lunar Planet. Sci. Conf., 265-266,* 1992.

Crisp, J., and S. Baloga, The influence of crystallization and entrainment of cooler material on the emplacement of lava flows, *submitted to J. Geophys. Res., 1993.*

Dingwell, D. B., and S.L. Webb, Structural relaxation in silicate melts and non-Newtonian melt rheology in geologic processes, *Phys. Chin. Miner., 16, 508-516,* 1989.

Dvorak, J. J., A.T. Okamura, T.T. English, R.Y. Koyanagi, J.S. Nakata, M.K. Sake, W.T. Tanigawa, and K.M. Yamashita, Mechanical response of the south flank of Kilauea Volcano, Hawaii, to intrusive events along the rift systems, *Tectonophysics,* 124, 193-209, 1986.

Einarsson, T., The flowing lava. Studies of its main physical and chemical properties, in *The eruption of Hekla 1947-1948,* edited by T, Einarsson, G. Kjartansson, and S. Thorarinsson,Visindafelg Islendinga, Reykjavik, Iceland, 1949.

Farris, R, J., Prediction of the viscosity of multimodal suspensions from unit-nodal viscosity data, *Trans. Sot, Rheol., 12,281-301, 1968,*

Fink, J, H., and J, Zimbelman, Longitudinal variations in theological properties of lavas: Puu Oo basalt flows, Kilauea Volcano, Hawaii, in *Lava flows and dorms. Emplacement mechanism and hazard implications,* edited by J.H. Fink, pp. 157-173, Springer-Verlag, New York, 1990,

Frankel, N. A., and A. Acrivos, On the viscosity of a concentrated suspension of solid spheres,

Chem. Eng. Sci., 22,847-853, 1967.

Gauthier, F., Field and laboratory studies of the rheology of Mount Etna lava, *Phil. Trans. R. Sot, London, Ser. A,* 274,83-98, 1973.

Gay, E. C., P.A. Nelson, and W.P. Armstrong, Flow properties of suspensions with high solids concentration, *AIChE J., 15,815-822,* 1969.

Ghiorso, M. S., Chemical mass transfer in magmatic processes, I. Thermodynamic relations and numerical algorithms, *Contrib. Mineral. Petrol., 90,* 107-120, 1985.

Ghiorso, M. S., and I.S.E. Carmichael, Chemical mass transfer in magmatic processes, II. Applications in equilibrium crystallization, fractionation and assimilation, *Contrib. Mineral. Petrol., 90, 121-141, 1985.*

Greenland, L. P., Composition of gases from the 1984 eruption of Mauna Loa Volcano, *U.S. Geol. Survey Prof. Paper 1.3.50,* pp. 781-790, 1987.

Guest, J.E., C.R.J. Kilburn, H. Pinkerton, and A.M. Duncan, The evolution of lava flow-fields: Observations of the 1981 and 1983 eruptions of Mount Etna, Sicily, *Bull. Volcanol., 49,527-*540, 1987.

Head, J. W., III., and L. Wilson, Volcanic processes and landforms on Venus: Theory, predictions, and observations, *J. Geophys. Res., 91,9407-9446,* 1986.

Helz, R. T., M. Mangan, K. Hen, and L. Simmons, Thermal history of the current Kilauean East Rift eruption, *EOS Trans. AGU, 72,557-558, 1991.*

Helz, R. T., and C.R. Thornber, Geothermornetry of Kilauea Iki lava lake, Hawaii, *Bull. Volcanol.,* 49,651-668, 1987.

Heslop, S, E., L. Wilson, H. Pinkerton, and J.W. Head, 111, Dynamics of a confined lava flow on Kilauea volcano, Hawaii, *Bull. Volcanol.,* .51,415 -432, 1989.

Hulme, G., and G. Fielder, Effusion rates and rheology of lunar lavas, *Phil. Trans. R. Sot. London, Ser. A,* 285,227-234, 1977.

Juster, T., M.J. Defant, and H. Jones, Stereological effects on crystal size distribution for orthorhombic and tetragonal crystals (abstract), *EOS Trans. AGU, 73, 620, 1992.*

Kataoka, T., T. Kitano, M. Sasahara, and K. Nishijima, Viscosity of particle filled polymer melts, *Rheol. Acts, 17, 149-155, 1978.*

Kerr, R. C., and J.R. Lister, The effects of shape on crystal settling and on the rheology of magmas, *J. Geology, 99,457-467, 1991.*

Kirkpatrick, R.J., Nucleation and growth of plagioclase, Makaopuhi and Alae lava lakes, Kilauea Volcano, Hawaii, *Geol.* Sot. *Am. Bull., 88,78-84,* 1977.

Kirkpatrick, R, J., Kinetics of crystallization of igneous rocks, in *Kinetics of geochemical processes,* edited by A.C. Lasaga and R.J. Kirkpatrick, Reviews in *Mineral., 8,321-398,* 1981,

Kitano, T., T. Kataoka, and T. Shirota, An empirical-equation of the relative viscosity of polymer melts filled with various inorganic fillers, *Rheol. Acts, 20, 207-209,* 1981.

Lipman, P.W., and N.G. Banks, Aa flow dynamics, Mauna Loa 1984, *U.S. Geol. Survey Prof. Paper 1350,* pp. 1527-1567, 1987.

Lipman, P. W., N.G. Banks, and J.M. Rhodes, Gas-release induced crystallization of 1984 Mauna Loa magma, Hawaii, and effects on lava rheology, *Nature, .317,604-607, 1985,*

Lockwood, J. P., N.G. Banks, T.T. English, L.P. Greenland, D.B. Jackson, D.J. Johnson, R.Y. Koyanagi, K.A. McGee, A.T. Okamura, and J.M. Rhodes, The 1984 eruption of Mauna Loa volcano, Hawaii, *EOS Trans. AGU, 66,169-171,* 1985.

Lockwood, J. P., J.J. Dvorak, T.T. English, R.Y. Koyanagi, A.T. Okamura, M.L. Summers, and W.R. Tanigawa, Mauna Loa 1974-1984: A decade of intrusive and extrusive activity, US. *Geol. Survey Prof. Paper 1.?.50,* pp. 537-570, 1987.

Mangan, M.T., Crystal size distribution systematic and the determination of magma storage times: the 1959 eruption of Kilauea volcano, Hawaii, *J. Volcanol. Geotherm. Res., 44, 295-302, 1990.*

Mangan, M, T., and Cashman, K., Vesiculation of basaltic magma during eruption - low energy versus high energy events (abstract), *EOS Trans. AGU, 73, 629,* 1992.

Mangan, M,T., K.V. Cashman, and S, Newman, Vesiculation of basaltic magma during eruption, Geology, *21,* 157-160, 1993.

Maron, S. H., and P.E. Pierce, Application of Ree-Eyring generalized flow theory to suspensions of spherical particles, *J. Colloid Sci., 11,80-95,* 1956.

Marsh, B.D., On the crystallinity, probability of occurrence, and rheology of lava and magma, *Contrib. Mineral. Petrol., 78,85-98, 1981.*

Marsh, B. D., Crystal size distribution (CSD) in rocks and the kinetics and dynamics of crystallization: I. Theory, *Contrib. Mineral. Petrol., 99,277-291, 1988.*

McBirney, A. R., and T. Murase, Theological properties of magmas, *Annual Rev. Earth Planet. Sci., 12,337-357, 1984.*

Metzner, A. B., Rheology of suspensions in polymeric liquids, *J. Rheol.,* 29,739-775, 1985.

Moore, H. J., Preliminary estimates of the theological properties of 1984 Mauna Loa lava, *U.S. Geol. Survey Prof. Paper 1350,* pp. 1569-1588, 1987.

Moore, H. J., and J.A. Ackerman, Martian and terrestrial lava flows, *20th lunar and Planet. Sci. Conf.,* pp. 711-712, 1989,

Murase, T., and A.R. McBirney, Properties of some common igneous rocks and their melts at high temperatures, *Geol. Sot. Am. Bull., 84,3563-3592, 1973.*

Murase, T., A.R. McBirney, and W.G. Melson, The viscosity of the dome of Mount St. Helens, .1. *Volcanol. Geotherm. Res., 24, 193-204,* 1985.

Naranjo, J.A., R.S.J. Sparks, M.V. Stasiuk, H. Moreno, and G.J. Ablay, Morphological, structural and textural variations in the 1988-1990 andesite lava of Lonquimay Volcano, Chile, *Geol. Msg., 129,657-678, 1992.*

Peck, D.L., Cooling and vesiculation of Alae lava lake, Hawaii, U.S. *Geol. Survey Prof. Paper, 93.5-B, 59 pp., 1978.*

Pinkerton, H., and R.S.J. Sparks, The 1975 sub-terminal lavas, Mount Etna: A case history of the formation of a compound lava field, *J. Volcanol. Geotherm. Res., 1, 167-182, 1976.*

Pinkerton, H., and R.J. Stevenson, Methods of determining the theological properties of magmas at sub-liquidus temperatures, *J. Volcanol. Geotherm. Res., .53, 47-66, 1992,*

Rhodes, J, M., Geochemistry of the 1984 Mauna Loa eruption: Implications for magma storage and

supply, *J. Geophys. Res.*, 93,4453-4466, 1988.

Russ, J. C., *Computer-assisted microscopy: The measurement and analysis of images*, pp. 216-217, Plenum Press, NY, 1990.

Russ, J, C., and T.M. Hare, Measurement of edge-intersecting features in SEM images, pp. 133-136, 20th *Microbeam Analysis Sot. Conf., 1985.*

Russell, J. K., Crystallization and vesiculation of the 1984 eruption of Mauna Lea, *J. Geophys. Res.*, 92, 13731-13743, 1987.

Ryerson, F.J., H.C. Weed, and A.J. Piwinskii, Rheology of subliquidus magmas I. Picritic compositions, *J. Geophys. Res.*, 93, 3421-3436, 1988.

Sate, K., K. Kashima, and I. Sunagawa, Measurements of nucleation rates and real growth rates of plagioclase in a solution of basaltic composition, J. *Japan. Assoc. Min. Petr. Econ. Geol., 76, 294-307, 1981.*

Schowalter, W. R., C.E. Chaffey, and H. Brenner, Theological behavior of a dilute emulsion, *J. Colloid Interface Sci., 26, 152-160, 1968.*

Shaw, H. R., Rheology of basalt in the melting range, *J. Petrol., 10,510-535,* 1969.

Shaw, H, R., Viscosities of magmatic liquids: An empirical method of prediction, Am. *J. Sci.*, 272, 870-893, 1972.

Shaw, H. R., and D.A. Swanson, Eruption and flow rates of flood basalts, in *Proc. 2nd Columbia River Basalts Symposium,* pp. 271-299, Washington State College Press, Cheney, WA, 1970.

Shaw, H. R., T.L. Wright, D.L. Peck, and R. Okamura, The viscosity of basaltic magma: An analysis of field measurements in Makaopuhi lava lake, Hawaii, *Am. J. Sci.*, 266, 22S-264, 1968.

Sibree, J. O., The viscosity of froth, *Trans. Faraday Sot., 30, 325-331, 1934.*

Smith, J.E., and M.L. Jordan, Mathematical and graphical interpretation of the log-normal law for particle size distribution analysis, *J. Colloid Sci., 19,549-559, 1964.*

Sparks, R. S. J., and H. Pinkerton, Effect of degassing on rheology of basaltic lava, *Nature, 276, 385-386, 1978.*

Spence, D. A., and D.L. Turcotte, Magma-driven propagation of cracks, *J. Geophys. Res.*, 90,575-580, 1985.

Spera, F. J., and D.J. Stein, Theological properties of martian magmas: Experiments and inferences (abstract), in *MEVTV Workshop on the evolution of magma bodies on Mars,* edited by P, Mouginis-Mark and J, Holloway, LPI Tech, Report 90-04, pp.54-55, 1990,

Spera, F. J., A. Borgia, J. Strimple, and M. Feigenson, Rheology of melts and magmatic suspensions, 1, Design and calibration of concentric cylinder viscometer with application to rhyolitic magma, *J. Geophys. Res.*, 93, 10273-10294, 1988,

Stasiuk, M. V., C. Jaupart, and R.S.J. Sparks, Influence of cooling on lava-flow dynamics, Geology, 21,335-338, 1993.

Stein, D. J., and F.J. Spera, Rheology and microstructure of magmatic emulsions: theory and experiments, *J. Volcanol. Geotherm. Res., 49, 157-174,* 1992.

Sundstrom, D. W., Viscosity of suspensions in polymeric solutions, *Rheol. Acts,* 22, 420-423, 1983,

Sura, V. M., and P.C. Panda, Viscosity of porous glasses, *J. Am. Ceram. Sot.,* 73,2697-2701, 1990.

Swanson, D. A., Pahoehoe flows from the 1969-1971 Mauna Ulu eruption, Kilauea Volcano, Hawaii, *Geol. Sot. Am. Bull., 6'4,615-626,* 1973.

Taylor, G., The viscosity of a fluid containing small drops of another fluid, *Proc. R. Sot. London, Ser. A, 1.78,41-48,* 1932.

Valko' and Economies, Volume equalized constitutive equations for foamed polymer solutions, *J. Rheol.,* 36, 1033-1055, 1992.

Wegner, M. W., and J.M. Christie, Preferential chemical etching of terrestrial and lunar olivines, *Contrib. Mineral. Petrol., 43, 195-212, 1974.*

Wegner, M,W., and J.M. Christie, General chemical etch ants for microstructure and defects in silicates, *Phys. Chem. Minerals, 12, 90-92, 1985.*

Wegner, M.W., R.E. Jones, and J.M. Christie, Exsolution in terrestrial and lunar plagioclases revealed by chemical etching, *Contrib. Mineral. Petrol., 65, 283-291, 1978.*

Wildemuth, C. R., and M.C. Williams, Viscosity of suspensions modeled with a shear-dependent maximum packing fraction, *Rheologica Acta, 23, 627-635*, 1984.

Wilson, L., and J.W. Head, III, Nature of local magma storage zones and geometry of conduit systems below basaltic eruption sites: Pu 'u' O'o, Kilauea east rift, Hawaii, example, *J. Geophys. Res.*, 93, 14785-14792, 1988.

Wright, T.L., and R.T. Okamura, Cooling and crystallization of tholeiitic basalt, 1965 Makaopuhi lava lake, Hawaii, *U.S. Geol. Survey Prof. Paper 1004,78* pp., 1977.

Wright, T.L., and D.L. Peck, Crystallization and differentiation of the Alae magma, Alae lava lake, Hawaii, *U.S. Geol. Survey Prof. Paper 93.5-C, 20* pp., 1978.

Appendix: CSD Data Collection and Analysis

Two CSD methods are needed to address the different aspects of lava-flow emplacement. The first provides growth and nucleation rates of plagioclase. These are useful for comparison with results from other experimental and CSD studies of plagioclase in basalt, such those done for the Hawaiian lava lakes [e.g., *Cashman and Marsh, 1988; Kirkpatrick,* 1977]. The second method, which provides crystallization rates averaged over all mineral types, is needed for estimating the increase in bulk viscosity and latent heat release as a function of distance downstream.

Method A: Point counts and Measurements of Long and Short Axes of Plagioclase

Backscatter SEM (BSEM) photographs were obtained from a JEOL-JXA-8600 Superprobe at Rutgers University. A CCD camera connected to an automated image-analysis-computing system provided digital images of the BSEM photographs. A Decision Images Processing unit was used at Princeton University to measure crystal dimensions. A mouse-driven cursor was used to

manually indicate endpoints of the long and short axes of about 250 plagioclase crystals in each sample. Although width measurements yield more accurate volume nucleation densities than length measurements [*Cashman*, 1992; *Juster et al., 1992],* length measurements are needed to determine maximum growth rates and are more sensitive indicators of changing conditions (Figure 7). The image-analysis software calculated and stored the crystal dimensions, which were later plotted in a 20-bin size-frequency histogram for CSD analysis. Crystals that intersected an edge of an image were not measured. Measurement errors for Method A are discussed in *Cashman and Marsh [1988],* and result in growth and nucleation rates with uncertainties of less than about one order of magnitude. For these same samples, point counts were made of crystals, glass, and vesicles in thin sections (500 points per thin section, 1 thin section per sample).

Method B: Crystal Area Measurements

This method used a CCD camera direct] y connected to a Nikon Optiphot microscope slid Analytical Imaging Concepts image-analysis computer system, This allowed capture of digital 512 x 480 pixel images with 256 shades of gray. Image analysis was done on 1-2 thin (or thick) sections per sample, for random] y selected microscope viewing frames. The number of frames analyzed per sample, for each of the different microscope objectives is given in Table 10. To optimize measurement of CSD's over a wide range of crystal sizes, only those crystals with a cross-sectional area falling in the range given in Table 10 were measured with each of the four microscope objectives. The data were combined for CSD analysis by giving the counts appropriate weights, according to the total area measured with each objective.

A mouse-driven cursor was used to manually outline the crystals on the display monitor, Measurements of crystal area, perimeter, length, and breadth were calculated and stored by the automated image-analysis software. Reflected light was used with all images taken with 40x and 10OX microscope objectives, Either reflected light on thick sections or transmitted light through ultrathin sections (< 10 μm thick) was used with the 5x and 10X objectives, Instead of making traditional point counts, the volume percent of crystals was taken directly from the image-analysis

measurements of the area percent of crystals.

Larger crystals are more likely to intersect the edge of an image frame and therefore more likely to be put in the wrong size bin in a histogram or CSD plot, To reduce this bias, only crystals not touching the frame edges were counted, and each crystal count was weighted according to its size in comparison to the size of the frame using the method proposed by *Russ [1990]* and *Russ and Hare* [1985].

Minimum uncertainties on crystal counts were calculated from statistical estimation theory for confidence intervals on proportions and propagation of errors. Assuming that the population of crystals in a sample is infinite and that an unbiased sample was selected, then the probability of a crystal falling into a specific size bin in a histogram is p and the probability that it does not is 1-p. Thus, a binomial distribution analysis was used to estimate the statistical errors, An estimate of p is given by the number of crystals counted per unit area in a specific size bin, divided by the total number of crystals counted per unit area for all the size bins. These uncertainties were used in further propagation of error calculations to determine the error bars on population density shown in Figure 4. These error bars represent minimum uncertainties at the 68% confidence level, because they do not include any estimates of systematic errors or errors inherent in the image analysis methods (e.g., pixel size effects, imprecise recognition of crystal grain boundaries, and operator bias).

Another approach to studying the errors involved is given in the results for two thin sections (95 and 95R1) taken from the same rock sample. The percentage of microphenocrysts in the two sections was estimated to be 20.8 and 21.7 and the percentage of microlites, 32 and 36 (Table 1). As shown in Tables 2 and 4, estimates of nucleation and growth rates for microphenocrysts and microlites measured in the two different thin sections were in agreement to within a factor of 4.

Figure Captions

Fig. 1. Map view of the 1984 Mauna Loa lava flow, modified from Fig. 57.1 B of *Lipman and Banks* [1987].

Fig, 2*a*. Backscatter secondary electron (BSEM) image (450 μm x 450 pm) of sample NER2, a near-vent sample collected 3 hours after the eruption began. Vesicles are round. Black crystals are feldspar microphenocrysts, gray crystals are pyroxene, some of which are patchy intergrowths or separate crystals of (dark gray) pigeonite and (light gray) augite. There is a minor amount of microlites and quench crystals. This image is not representative of the 11% crystal abundance of NER2, but the cluster of crystals features the two pyroxenes.

Fig, 2*b*. BSEM image (450pm *x* 450 μm) of sample NER1 2/65, near-vent sample collected 467 hours after the eruption began, Same types of crystals as in Figure *2a,* but no individual pigeonite crystals.

Fig. 3. Crystal-size distribution for postemplacement sample 68c. Size measurements (equivalent circular diameter) were made for all minerals in the sample (Method B in Appendix). The five smallest bins are results for microlites, and the rest are for microphenocrysts.

Fig. 4. Natural logarithm of population density n versus crystal size *L,* The example is for all the crystals (plagioclase, pyroxene, and olivine) in sample 68c. The two diagonal lines are separate least-squares fits for the microlites (< 20 pm) and microphenocrysts (>20 pm), weighted according to $1/\sigma_i^2$. Error bars show $\pm \sigma_i$ for each (ith) estimate of in(n), where σ_i is one standard deviation (see Appendix for details).

Fig. 5. Volume percent microphenocrysts in near-vent samples, as a function of time. * and x measurements are from Figure 57.25 in *Lipman and Banks [1987].* Sample type information (perched lava pond, spatter, aa, or pahoehoe) was provided by J. Lockwood.

Fig. 6. Nucleation density of microphenocrysts in near-vent samples, as a function of time. Data point at 0.5 hrs, 30000 microphenocrysts per μm^2, was removed from the plot to enhance general trend with time. Each data point is the average for a sample. +'s are for all the microphenocrysts (plagioclase, pyroxene, and olivine) in a sample. Box-X's are for just plagioclase, and are slightly biased higher than actual values because they were measured from BSEM photos that were preferentially taken in areas with more abundant crystals.

Fig. 7. Average long and short axes of plagioclase microphenocrysts in near-vent samples, as a function of time. Sizes were averaged for each sample (average size on a volume-weighted basis is $3G\tau$ *[Marsh,* 1988]).

Fig, 8. Growth rate of near-vent microphenocrysts as a function of time, Each data point represents the average for an individual sample.

Fig. 9. Nucleation rates of near-vent microphenocrysts as a function of time. Squares represent combined estimates of plagioclase and pyroxene, diamonds and *'s are for plagioclase only.

Fig, 10. Eruption temperature based on glass composition, as a function of time at the vent, Temperatures were calculated from CaO and MgO concentrations, using the relationship developed for Kilauea basalts by *Helz and Thornber [1 987]*. Calculations do not account for the slight differences in composition between the Kilauea and Mauna Loa magmas. Glass compositions were determined on the Rutgers University JEOL-JXA-8600 Superprobe. One standard deviation (σ) error bars are shown, calculated from the standard deviations on the probe analyses. The CaO temperatures have less error (+20=$\pm 6^{o}$C) than the those from MgO ($\pm$1 O"C).

Fig. 11. Thermodynamic equilibrium predictions for crystal abundances in a magma that has a bulk chemical composition equal to that of the Mauna Loa 1984 lavas *[Rhodes,* 1988]. Equilibrium crystal abundances were calculated using the methods of *Ghiorso [1985]* and *Ghiorso and Carmichael [1985].* The trail of solid arrows indicates the approximate temperature/crystalli zation path actually followed by the Mauna Loa lavas.

Fig. 12. Contours of roughl y equal elevation have been drawn on this plot of apparent viscosity versus time, based on elevations of the locations where *Moore [1987,* Fig. 58,14] estimated apparent viscosity for different times during the Mauna Loa flow emplacement. A region is shown for the dates and viscosity estimates of *Moore [* 1987] for the vents at 2850-2870 m elevation. Error bars show values interpolated from *Moore's [1987]* estimates, based on the elevations and dates of collection for samples NER1 2/27 (1753 m elevation, March 30), 12/48(1935 m, April 6), and 12/ 57 (2225 m, April 8). Circles show our estimates of crystal-melt suspension viscosity for the same three samples, using Equation (5) and melt viscosities in Table 6 (minimum and maximum estimates are given for NER1 2/27, for $0.5 < \Phi_m < 0.6$).

Fig, 13. Viscosity of a crystal-melt suspension as a function of volume fraction of crystals, predicted by the equation for η_{susp}/η_{melt} of *Frankel and Acrivos* [*1967]* and η_{melt} from Table 6,

TABLE 1. Crystal Measurements for Near-Vent and Postemplacement Samples

Sample[b]	Hours since start of eruption	Total% crystals	Microphenocrysts[a] %	Microphenocrysts[a] x	Microphenocrysts[a] N/A	Microlites[a] %	Microlites[a] x	Microlites[a] N/A	CSD Method[c]
Near-vent Quenched Samples									
MOK3	0.5				3X10"4				A
MOK7	1.3	23			1X1 0-4				A
NER2	3.33	11			6×10^{-5}				A
NER6	6.75	23			1X1 0-4				A
NER1O	8,50	27,5			8×10^{-5}				A
NER12/3	35.92	9.5	6.7	38	5X1 0-5	2.8	13	1×10^{-4}	B
NER12/7	55.00	14.5	9.8	37	7X1 0-5	4.7	9	7X10"4	B
NER12/9	58.35				5X10"5				A
NER12/19	79.58	31			7X10"5				A
NER12/21	87,17	30			5X1 0-5				A
NER12/23	112,83	22.0	20.4	49	8X10-S	1.6	11	7X1 O-5	B
NER12/24	125.93	28			6x1 O-S				A
NER1 2/28	155.25	21.8	19.6	44	9X1 O-5	2.2	12	1X1 O-4	B
NER1 2/35	208.25				3X1 O-5				A
NER1 2/46	297.00	13.2	13.2	49	6X10-S	0			B
NER1 2/56	350.83	16.9	15.4	58	4X1 0^{-5}	1.5	15	9X1 O-5	B
NER12/64	464.58	21.8	20,4	57	6x1 O-S	0.6	11	3X1 O-5	B
NER1 2/65	467.25				5×10^{-5}				A
NER1 2/66	488.75	21,8	21.3	58	7X1 O-5	0.5	4	3X1 O-4	B
NER12/67	515.75	34.5			3×10^{-5}				A
Postemplacement Samples Collected in 1987									
95		57.3	21.7	46	7X10-^{5}	35.6	6	9 x 10^{-3}	B
95R1		53.2	20.8	47	1X10^{4}	32.4	5	1×10^{-2}	B
107		58.1	18.4	59	8×10^{-5}	39,7	5	1 x 10"^{2}	B
70a		58,1	23.8	41	3X1 O-3	34.3	10	3×10^{-3}	B

72b	53	16.7	26	1X1 0-4	36.2	7	7x10 ^{3}	B
68C	56	19,4	36	1X10-^{4}	36.7	7	7 x 10 $^{-3}$	B

[a] % = volume percent, x = average grain size (pm), N/A = number of crystals per μm^2.

[b] MOK3, MOK7, NER2, NER6, and NER1 O: cold spatter, NER1 2/3: water-quenched, NER1 2/7: water-quenched spatter, NER1 2/9: air- and water-quenched spatter, NER 12/19: water-quenched pahoehoe bud from base of perched lava pond, NER1 2/21: water-quenched pahoehoe bud from overflow from base of pond, NER1 2/23: water-quenched pahoehoe in perched pond, NER1 2/24: pahoehoe bud from middle of lava pond, NER1 2/28: water-quenched pahoehoe from tumulus on edge of perched lava pond, NER1 2/35: spatter, NER1 2/46: water-quenched spatter, NER1 2/56: water-quenched scoop from channel, NER1 2/64: water-quenched fluff from channel, NER1 2/65: water-quenched channel overflow from surge, *50 m* from main channel, NER1 2/66: pahoehoe tube at distal end of pahoehoe overflow 150 m long, NER1 2/67: air-cooled spatter, 95: upper part of fourth unit from the top of a sequence of 14 channel spill over units, 9.5 km from vent, 95R1: same as 95, different thin-section, 107: same location as 95, top of the lowermost exposed spill over unit, 70a: flow margin of the 1 flow lobe, 12 km from vent, 72b: channel of 1A lobe, 12 km from vent, 68c: center of 1 A channel, 20 km from vent.

[c] CSD methods in Appendix.

TABLE 2, Growth and Nucleation Rate Information for Microphenocrysts

sample[a]	crystals[b]	n^o (cm^{-4})	G-c (cm)	G^*(cm S-l)	J^*(cm^{-3} s^{-1})
MOK3	plag[L]	1.9X10[9]	1,2X10"3	6,6X1 O-7	1300
MOK7	plag[L]	2,4x10[8]	2.8x10[-3]	5,9X1 O-7	140
MOK7	plag[S]	2.1X10[9]	4.5X104	9.4X10"8	190
NER2	plag[L]	1.1×10[8]	2.5x1 0[-3]	2,1 X1 O-7	22
NER2	plag[S]	2.6x10[8]	3.4X1 O-4	2.9x1 0[-8]	7.4
NER6	plag[L]	2$1X108	2.7x10[-3]	1.1 X1 O-7	23
NER6	plag[S]	1.3X109	5,1X10[4]	2.1 X1 O-8	27
NER1O	plag[L]	1.3×10[8]	3.3 X1 O-3	1.1 X1 O-7	13
NER1 O	plag[S]	1 .0×10[9]	4.9X104	1.6x10[-8]	16
NER1 2/2	plag[L]	2.1X108	3.3X1 O-3	2.6x1 0[-8]	5 . 6
NER1 2/2	plag[S]	1.2X109	6.4x1 0[-4]	5.2x10[-9]	6.4
NER1 2/3	average	5, OX108	2.4x1 0[-3]	1.8x1 O-S	9.2
NER1 2/7	average	6.6X1 0[8]	2.2X10"3	1.1 X1 O-8	7.4
NER1 2/9	plag[L]	5. OX107	4.4X1 0[-3]	2,1 X10"8	1.0
NER1 2/9	plag[S]	5.2x10[8]	6.8X104	3.2x10[-9]	1.7
NER12/19	plag[L]	5.9X107	5.2x10[-3]	1.8x10[-8]	1.1
NER12/19	plag[S]	8.3x10[8]	6.5x 10[-4]	2.3x1 0[-9]	1.9
NER1 2/21	plag[L]	5.9X107	4.3 X1 O-3	1.4X1 0[-8]	0.81
NER1 2/21 ·	plag[S]	1.5X109	6.1x10[4]	2. OX10-9	2.9
NER1 2/22**	average	2.0×10[9]	2.1 X1 O-3	5.2x10[-9]	10
NER1 2/23	average	2,0X10[9]	2,9X1 O-3	7.1 X1 O-9	14
NER1 2/24	plag[L]	3.8x10[7]	5,5X1 O-3	1,2X1 O-8	0.46
NER1 2/24	plag[S]	5.5X108	7.8x10[4]	1.7X1 O-9	0.95
NER1 2/27""	average	3.2x10[8]	3. OX10"3	5.3X1 O-9	1,7
NER1 2/28	average	8.6X108	2,7x10[-3]	4.8x10[-9]	4,1

NER1 2/35	plag^{L}	I,6x10^{7}	5,7X1 O-3	7.6x10^{-9}	0.12
NER1 2/35	plag^{S}	9,4X107	1.1 X1 O-3	1,5X1 O-9	0.14
NER12/46	average	2.5x10^{8}	3.2x10^{-3}	3, OX1O-9	0.77
NER12/48**	average	2,6x10^{8}	301 X10-3	2,9x10-^{9}	0.75
NER1 2/56	average	3.8x10^{8}	3,8x10^{-3}	3. OX1O-9	1.1
NER12/57**	average	2$_{0}$0X108	3.3X1 O-3	2,6x1 0^{-9}	0,52
NER1 2/64	average	1,6x10^{8}	5.4X1 0^{-3}	3.2x10-^{9}	0,52
NER1 2/65	plag^{L}	1.5X107	7.6x10^{-3}	4.5X1O"9	0,069
NER1 2/65	plag^{S}	1,9X108	1,1 X1 O-3	6,7x10^{-1}^{0}	0.13
NER12/66	average	1.7X109	3.6x10^{-3}	201 X10-9	3.5
NER1 2/67	plag^{L}	1.2X107	7.2x10^{-3}	3.8x10-^{9}	0,047
NER1 2/67	plag^{S}	2,3x10^{8}	9.5X10^{4}	5.1 X1O-10	0,12
NER1 2/22'	plag	4,4X108	3.4X1 O-3	8.6X1 O-9	3.7
NER1 2/22'	pxol	3.2x10^{8}	2,4x10^{-3}	6.2x1 0^{-9}	2.0
NER12/27d	plag	2.2X108	2.9x1 0^{-3}	6. OX1O-9	1.3
NER12/27d	pxol	1.7X108	2.2X1 O-3	4.6x10-^{9}	0.78

Postemplacement samples (τ is unknown) :

68 C**	average	1.7×10^{9}	2.3x1 0^{-3}
70A**	average	1.8x10^{9}	109X10-3
72B**	average	1.6x10^{9}	1.8x1 O-3
95R1**	average	8.9x10^{8}	2.6x10^{-3}
95"*	average	3.4X108	3.3X1 O-3
107**	average	3.1X108	3.3X1 O-3

*G and *J* were calculated assuming that τ is the time interval between onset of eruption at 0100 March 25 and sample collection.

**Samples collected far from the vent.

[L] = long axis of crystals viewed in BSEM image (Method A), s = short axis of crystals viewed in BSEM image (Method A).

[a]Samples are described in Table 1 footnote, or here. NER 12/2: water-quenched hot spatter from near the vent, collected 34.67 hours after the beginning of the eruption, NER1 2/22: part water-quenched aa ovefflow, NER12/27: air-quenched icicle on thermocouple, outbreak from aa flow, NER1 2/48: water-quenched mobile aa core, ovefflow from main aa channel, NER1 2/57: water-quenched overflow from main channel.

[b]plag = plagioclase (Method B), pxol = pyroxene and olivine (Method B), average = average of all the rnicrophenocrysts (plagioclase, pyroxene, and olivine, Method B),

[c]NER 12/22 has 9% plagioclase and 6% pyroxene + olivine microphenocrysts.

'NER 12/27 has 9% plagioclase and 4% pyroxene + olivine microphenocrysts.

TABLE 3, Near-Vent Versus Far-Vent Samples (Quenched Dip Samples)

Date	Distance from vent (km)	Sample	Total % crystals	Microphenocrysts[a]			Microlites[a]		
				%	x	N/A	%	x	N/A
3/29	O	NER1 2/23	22	20.4	49	8×10^{-5}	1.6	11	7×10^{-5}
3/29	9	NER12/22	59	15,1	39	9×10^{-5}	44,0	5	1×10^{-2}
3/31	0	NER12/28	22	19.6	44	9×10^{-5}	2,2	12	1×10^{-4}
3/30	14	NER12/27	39	13.7	47	7×10^{-5}	25.3	6	7×10^{-3}
4/6	o	NER1 2/46	13	13,2	49	6×10^{-5}	o		
4/6	11	NER1 2/48	24	9,0	54	6×10^{-5}	15.1	5	7×10^{-3}
4/8	o	NER1 2/56	17	15.4	58	4×10^{-5}	1.5	15	9×10^{-5}
4/8	6	NER12/57	22	9.0	52	5×10^{-5}	13.3	4	8×10^{-3}

[a] % = volume percent, x = average grain size (pm), N/A = number of crystals per μm^2. All measurements made using Method B (Appendix). Sample descriptions in footnotes to Tables 1 and 2. Estimates of x and N/A for microlites are highly uncertain, due to the very small number of microlites counted in these near-vent samples. A large fraction of the microlites in sample NER 12/22 may have formed after the sample was removed from the channel, because the sample was only partially quenched.

TABLE 4. Growth and Nucleation Rate Information for Microlites in Samples Collected During Eruption (NER Samples) and Postemplacement

sample[a]	n^o (cm^{-4})	$G\tau$ (cm)	-c* (rein)	G (cm s^{-1})	J (cm^{-3} s^{-1})
NER12/22pxb	4.2x10^{12}	3,4X104	*70*	8,1x10-S	*3.4X1 0^5*
NER 12/22plagb	1, 0×10^{12}	5.7X1 O-4	*70*	1.3X1 O-7	*1.4X105*
NER12/57px	1.7X1012	2.9x1 0^{-4}	100	4,8x 10-8	*8.4x10^4*
NER12/57plag	6.6×10^{11}	4.2x10^4	100	7. 0X10-8	*4.6x10^4*
NER12/48px	1.7×10^{12}	3.5X1 O-4	110	5.3X1 O-8	*9,2x10^4*
NER12/48plag	5. 0×10^{11}	4.6x1 0^{-4}	110	6,9x10^{-8}	*3.5X104*
NER12/27pxc	1.5×10^{12}	3.7X104	230	2.7x10^{-8}	*4. 0X104*
NER12/27plag	1.7×10^{11}	7.8x10^4	230	5.6x10-^{8}	*9.6x1 0^3*
68 Cplag	1.3×10^{11}	1.4X1 O-3			
68Cpx	8.9×10^{11}	5.6×10^{-4}			
70Aplag	1.3×10^{11}	9.1 X1 O-4			
70Apx	2.7×10^{11}	6.5x1 0^{-4}			
72Bplag	1.8×10^{11}	1.3X103			
72Bpx	1.7×10^{12}	4.1X104			
95plag	6.2x10^{12}	3,6x10^4			

95px	1.2×10^{12}	$5_0$7X 104
95R1plag	$1_0$5X10^{12}	$5_0$5X10^{4}
95R1px	$4,0\times10^{12}$	3.7X1 0-4
107plag	5,9X10^{11}	6.6X10^{4}
107px	5,2x10^{12}	3.0X1O4

[a]plag = plagioclase, px = pyroxene, sample descriptions in Table 1 footnote. All measurements made using Method B (Appendix).

[b]NER1 2/22 has 22% plagioclase microlites and 22% pyroxene microlites. A large fraction of these microlites may have formed after the sample was removed from the channel, because the sample was onl y partially quenched,

[c]NER 12/27 has 13% plagioclase and 12% p yroxene microlites.

*Surface flow velocities, $v_{surface}$, in the channel can be obtained from Table 52.3 in *Lipman and Banks* [1987]. *Moore* [1987] estimated that average flow velocities in the channel were roughly 1/2 to 2/3 those at the surface. Thus, estimates of crystal growth time are estimated from -c= $v_{surface}$ / 2 d, where d is the distance between the vent and site of quenching, and $v_{surface}$ is taken from measurements [Lipman and Banks, 1987] that were made along the flow at the same or nearly the same date as the samples were collected,

TABLE 5. Shear Rate, Vesicularity, Capillary Number (*Ca*), and Time Scale for Viscous Deformation of Bubbles (τ_b^{-1})

	Shear rate[a] (s-l)	Volume% Vesicles[a]	*Ca**	τ_b^{-1} *
Mauna Loa flow				
March 25-26, near vent	0,005-1	55-65	*0.0007-1*	1-7
April 2, stable channel near vent	6	55-75	*1"5*	*1-6*
April 13, near vent	0.3	70-80	*0.06 -0.3*	1-5
April 6-8,6-11 km downstream	0.3 to 0.6	35-50	0.2-1	1-5
March 30, 14 km downstream	0,2	≈ 25	≈ 0.3 - 8	1-5
April 2-3, 26 km downstream	≈ 0.0006	≈ 1-1o	10-50	0.3-2
Laboratory Experiments on Rhyolite				
Stein and Spera [1992]	*0.06-7*	*0.8- 5.5*	10-80	*0.02-0.25*
Bagdassarov and Dingwell [1992]	10-7- 10-5	*5-68*	*1-60*	*103-104*

'Rough estimates of shear rate were obtained by dividing surface centerline flow velocity by flow thickness [data in *Lipman and Banks,* 1987; *Moore,* 1987]. Local shear rates in a Newtonian flow would be twice as high at the base, and zero at the center of the top surface [*Heslop et al., 1989],* Shear rates would be lower in a Bingham flow. Vesicularity is estimated from bulk density measurements of quenched samples in *Lipman and Banks [1987],* assuming a magma density of 2600 kg m^{-3}.

*Capillary number *Ca* and τ_b^{-1} were estimated assuming that most of the vesicularity was included in 1-5 mm bubbles, as found in Kilauea lavas [*Cashman et al.,* 1992; *Mangan and Cashman,* 1992; *Mangan et al., 1993].* For laboratory experiments, measured mean bubble size was used. Although not strictly valid, crystal-melt suspension viscosity was used instead of melt viscosity in the equations for *Ca* and τ_b^{-1}.

TABLE 6. Interstitial Glass Composition of the 1984 Mauna Loa Lava in Samples with a Crystal Volume Fraction of Φ, and Estimated Melt Viscosities

	ML-156[a,b]	ML-176[a,b]	ML-210[a,b]	NER1 2/27[a,c]	Simulation[ad]
SiO_2	52.19	52.52	53.75	51.88	54.82
TiO_2	2,11	2.29	2.65	2.98	4.57
Al_2O_3	13,94	13.43	12,95	12,37	11,62
Fe_2O_3	1,64	1,74	1.92	2.25	2,81
FeO	9.31	9.88	10.88	12,78	15.92
MnO	0.17	0,19	0.20	n.d.	0.27
MgO	6.57	6.17	5.48	4.42	0.72
CaO	10,58	10.43	9.78	9,04	5.29
Na_2O	2.55	2.57	2.36	2.38	3.35
K_2O	0.38	0.41	0.47	0.59	0.91
Φ	o	10	*30*	*39*	*60*
T (°C)[e]	1140	1140	1137	1126	1115
Viscosity of the melt (Pas)	[f] 91	96	130	119	385

'Analyses have been normalized to 100% total, with wt% H_2O set equal to 0.1. Viscosity estimates are not very sensitive to differences of 0.1 % H_2O, and wt% H_2O in the Mauna Loa lavas was less than about 0,2 *[Russell,* 1987; *Lipman and Banks, 1987].* Weight% ratio of $Fe_2O_3/(Fe_2O_3 + FeO)$ was set equal to 0.15.

[b]Microprobe analyses from *Rhodes [1988].*

[c]Average of 20 anal ysis measured in one thin section using the Cameca SX-50 electron microprobe at the University of Oregon.

'This simulation is a calculation of the average 1984 magma minus 5% olivine, 27.5910 plagioclase, and 27.5% clinopyroxene, having mineral compositions as shown in Table 4 in *Rhodes [1988].* This rough calculation does not take into account changing phase compositions and the presence

of orthopyroxene microphenocrysts.

'Temperatures for ML- 156 and ML- 176 are estimates from vent temperatures [*Lipman and Banks, 1987]*. Temperatures for ML-21O and Simulation are estimates from Figure 11, Temperature for NER12/27 was measured in the field at the time of sample collection [*Lipman and Banks*, 1987].

fMelt viscosities calculated using the method of *Shaw [1972]*, at the temperatures shown,

TABLE 7. Crystal-melt Suspension Viscosity of Sample NER 12/27 (Φ = 0.39), Predicted by Different Equations for $\eta_{susp} / \eta_{melt}$

	Suspension Viscosity[a] (Pas)			
Φ_m	Eqn (I)[b]	Eqn (11)[c]	Eqn (lII)[d]	Eqn (IV)[e]
0.44	3200	9200	45000	27000
0.5	1500	2500	4300	5200
0.6	860	980	1100	1600

[a]Suspension viscosity, η_{susp}, calculated from four different equations (Equations (I)-(IV)), using η_{melt} = 119 Pas, from Table 6.

'Equation (I) derived from theory (not empirical) [*Frankel and Acrivos, 1967; Metzner, 1985]:*

$$\frac{\eta_{susp}}{\eta_{melt}} = \frac{9}{8}\left[\frac{(\Phi/\Phi_m)^{1/3}}{1-(\Phi/\Phi_m)^{1/3}}\right]$$

[c]Equation (11) from *Maron and Pierce [1956], Kataoka et al. [1978], Kitano et al. [1981],* Sundstrom [1983], and Metzner [1985]: $\frac{\eta_{susp}}{\eta_{melt}} = \left[1-\left(\frac{\Phi}{\Phi_m}\right)\right]^{-2}$

'Equation (III) for high shear rates from *Gay et al.* [1969]: $\frac{\eta_{susp}}{\eta_{melt}} = \exp\left[2.5\left(\frac{\Phi}{\Phi_m-\Phi}\right)^{0.48}\left(\frac{\Phi}{\Phi_m}\right)\right]$

'Equation (IV) for low shear rates from *Gay et al. [1969]:* $\frac{\eta_{susp}}{\eta_{melt}} = \left(\frac{\Phi_m}{\Phi_m-\Phi}\right)^{2.5}$

TABLE 8. Yield Strength Estimates for Crystal-Rich Samples

	Yield Strength τ_y (Pa)		
	NER12/57 Φ=0.22	NER 12/48 Φ=0.24	NER12/27 Φ=0.39
Moore [1987]'	$10^{2.5}$ to 10^3	102"5 to 103	10^3 to $10^{3.5}$
Shaw et al. [1968][b]		70-120	
Ryerson et al. [1988]"	87	110	440
Spera and Stein-high shear[d]	75	95	350
Spera and Stein-low shear[d]	4	5	28
Gay et al. [1969]'	0.2 to 0.5	0.3 to 0.5	1.2 to 1.6

[a]From measurements of flow dimensions and slope of the Mauna Loa flow, made on April 3, at similar distances from the vent as samples NER1 2/57, 12/48, and 12/27. Unlike the laboratory experiments, these τ_y's include the effects of solid lava chunks and bubbles.

[b]Yield strength of Hawaiian tholeiite with 25% crystals and less than 10% bubbles, from laboratory viscometer measurements at shear rates of about 0.1 to 1 s-l.

[c]Power law fit of laboratory measurements of picrite basalt at shear rates of 25- 170s-^{1} gives $\tau_y = 6500\,\Phi^{2.85}$,

'Unpublished report by F.J. Spera and D.J. Stein, presented at the MEVTV workshop on the Evolution of Magma bodies on Mars, San Diego, CA, Jan 15-17, 1990. From an analysis of published laboratory measurements, they recommend using these equations for basaltic and andesitic magmas: τ_y = 75003"5 for shear rates between 0.01 and 1 s^{-1}, and $\tau_y = 4500\,\Phi^{2.7}$ for shear rates of 1 to 200s-^{1}.

'Equation in *Gay et al. [1969]* and discussed in *Pinkerton and Stevenson* [1992]:

$\tau_y = 3.14\text{X}\,10^{-2}\left(\frac{D_p}{\Phi_m - \Phi}\right)\left(\frac{\Phi_m}{1-\Phi_m}\right)^2\left(\frac{1}{\xi^{1.5}\sigma_g}\right)$, where τ_y is in Pa, D_p is geometric mean particle diameter in μm, σ_g is a dimensionless geometric standard deviation as defined in Pinkerton

and Stevenson [1992], and ξ is a crystal shape factor, This is equivalent to equation (27) in *Gay et al. [1969],* with a conversion in units. Yield strengths shown in the table span the range for Φ_m = 0.44 to 0.6. Input parameters used were ξ = 0.7 (shape parameter for rods with 3:1:1 aspect ratio), for NER12/57: D_p = 3.74,08 = 1.52, for NER12/48: D_p = 3.99, σ_g = 1.56, and for NER12/27: D_p = 4.89, σ_g = 1,43. D_p and σ_g were calculated from the crystal-size counts using Equations 5 and 6 in *Smith and Jordan [1964].* The yield strength estimates are similar when σ_g is calculated using Equation 9 in *Smith and Jordan [* 1964]. The *Smith and Jordan* [1964] equations and the *Gay et al. [1969]* equation for yield strength are strictly valid only for particles with log-normal size distributions.

TABLE 9. Heat Released From the Inner Core (Joules per Gram of Lava)

Type of heating	first 5 days 26 km flow length	first 12 hours 11 km flow length
Heat of crystallization in the channel'	+ 87 to + 157	+ 87 to + 157
Viscous heating[b]	+2 to +8	+ 4 to + 12
Radiation of exposed core'	-0.6 to -70	-0.3 to -22
Convection of exposed core[d]	-0.03 to -4	-0.02 to -1.3
NET HEAT CHANGE PREDICTED	+ 15 to + 164	+68to+ 169

'Assuming an average of 350 Joules of latent heat per gram crystallized, average of 25-45% crystallization during emplacement.

[b]A rough estimate of viscous heating due to shear along the base of the flow, using an equation for Newtonian laminar flow in a rectangular channel: viscous heat per gram = $g \sin\alpha$ Q L $\Im$ / 2 *V,* where Q, is average volume flux through the channel (between 2 x 10^5 and 1 x 10^6 $m^3 hr^{-1}$ for first 5 days, 5 x 10^5 and 1.5x 10^6 $m^3 hr^{-1}$ for first 12 hours), *L* is flow length, $\Im$ is emplacement duration, g is gravity, α is average slope (4° for first 5 days, 4.7° for first 12 hours), and *V is* total volume (about 1.3 x 10^8 m^3 for first 5 days, 2.1 x 10" m^3 for first 12 hours) [*Lipman and Banks,* 1987; *Moore,* 1987].

[c]Estimated using the two-component thermal model of Crisp *and Baloga [1990],* for an average fraction of exposed core (*f*) of 0.2% to 10% for the entire flow, average *f* between 1% and 30% for the first 12 hours, and core temperature between 1110 and 1140°C.

'Calculated surface heat flux by natural convection using $H (T_{surface} - T_{air})^{5/4}$ with a convection heat coefficient H = 2 J $K^{-5/4}$ m^{-2} s^{-1} [*Carslaw and Jaeger,* 1959, p.21], T_{air} = 25°C, $T_{surface}$ between 1140 and 11 10°C (from exposed hotter core measurements in *Lipman and Banks [1987],* and same fraction of exposed core as in footnote c.

TABLE 10. Crystal Measurement Parameters for Four Different Microscope Objectives Using Method B.

Microscope objective	Area of individual crystals (μm^2)	Imaging frame area (mm^2)	Number of frames measured per sample
5 x	*>6400*	*2.0*	*6-8*
lox	*400-6400*	*0.5*	*4-12*
40x	*25-400*	*0.03*	*4-9*
loox	1-25	0.005	4-8

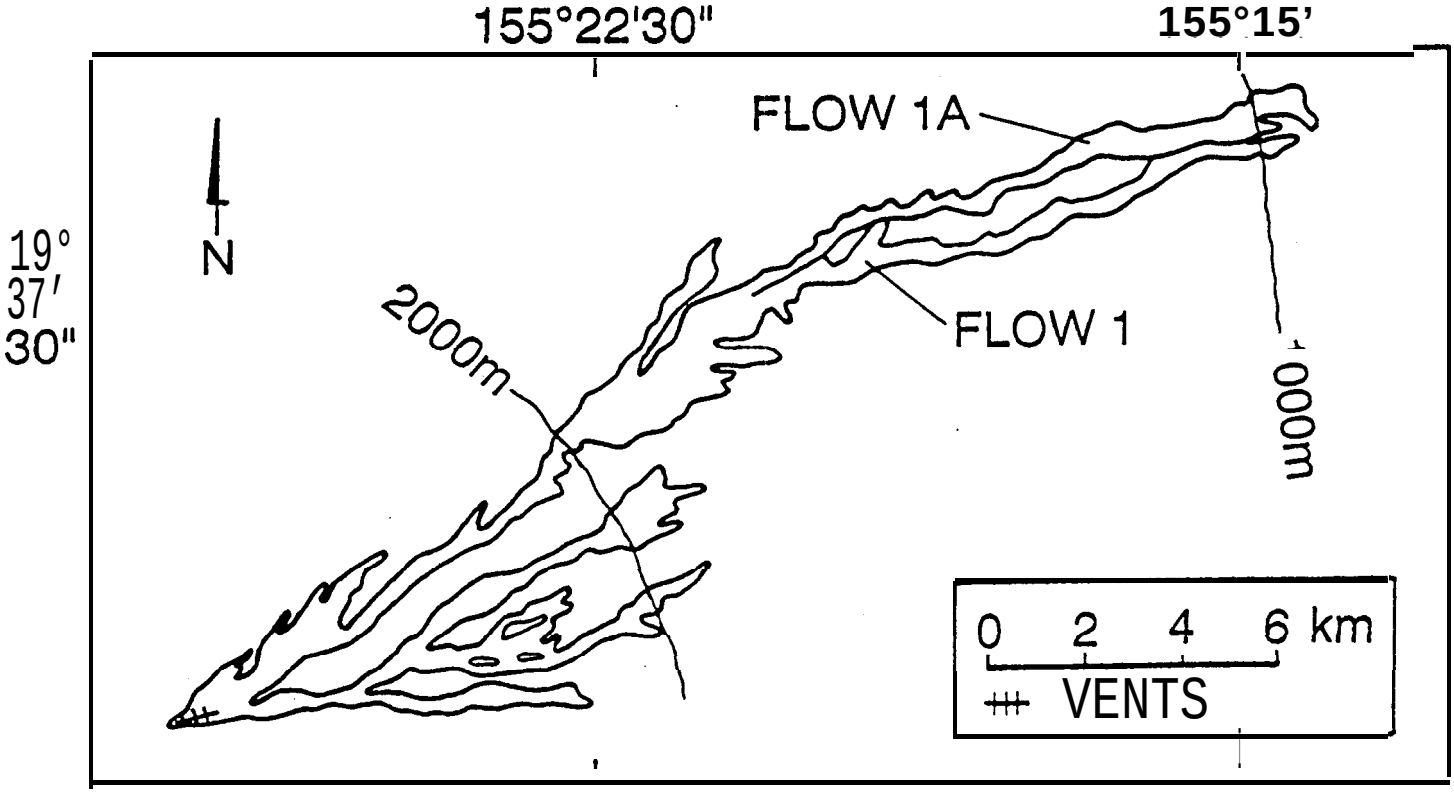
155°22'30"
155°15'
19°
37'
30"
N
FLOW 1A
FLOW 1
2000m
000m
0 2 4 6 km
VENTS

Fig. 1

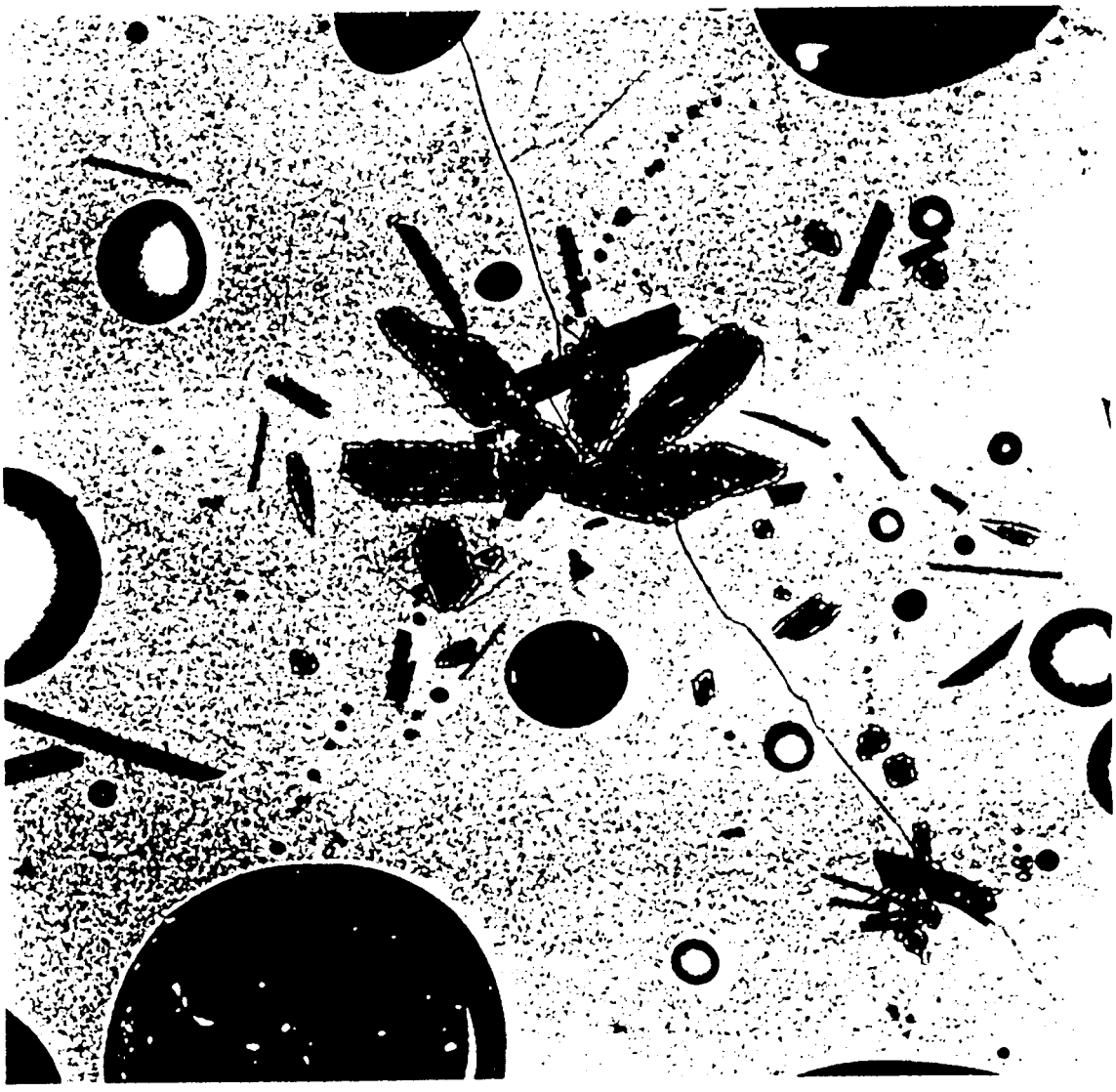

Fig.2a

Fig. 2b

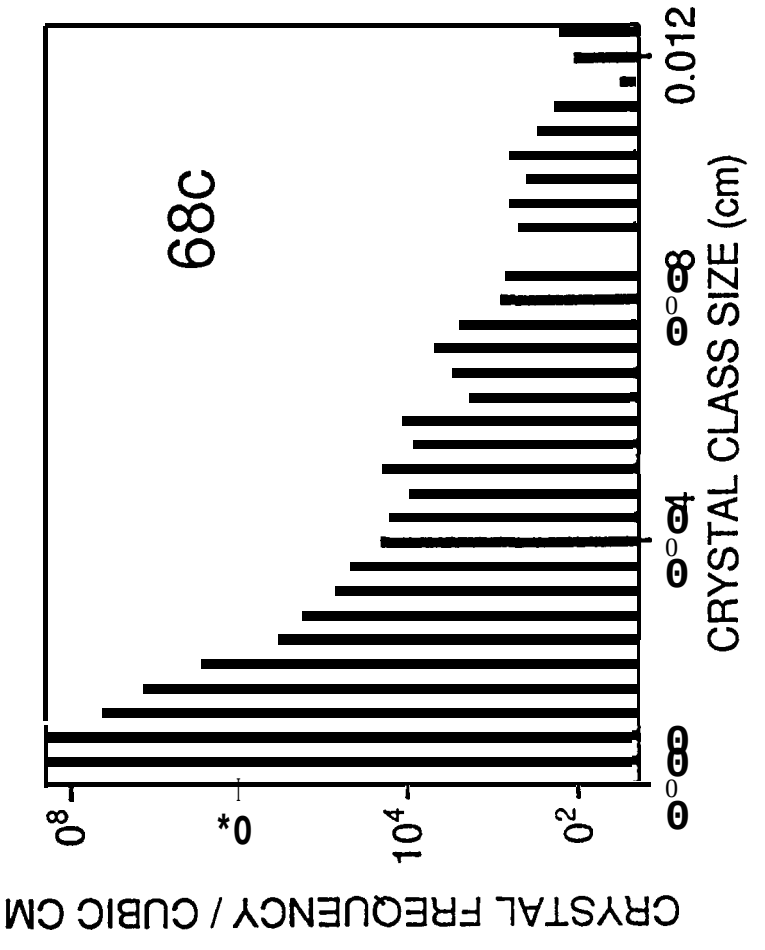

Fig 3

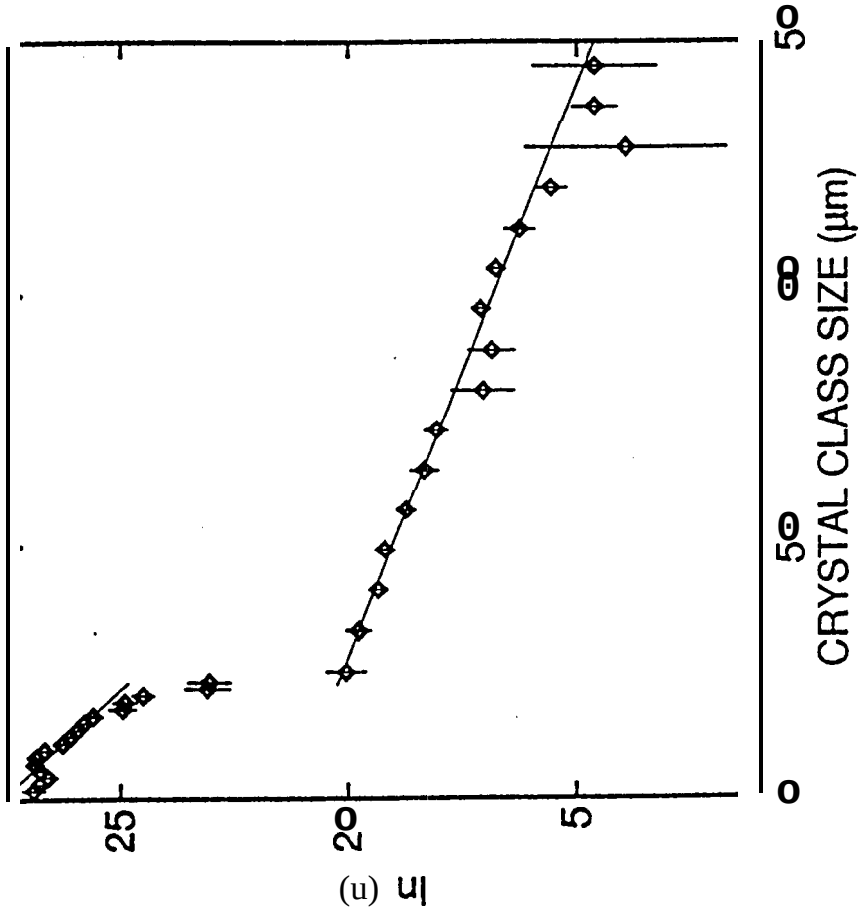

Fig. 4

VOLUME PERCENT CRYSTALS
0
20
0
100
200
300
400
500
TIME SINCE ERUPTION START (hrs)
* spatter, aa, pahoehoe
× perched lava pond
◇ Table 1 measurements

Fig. 5

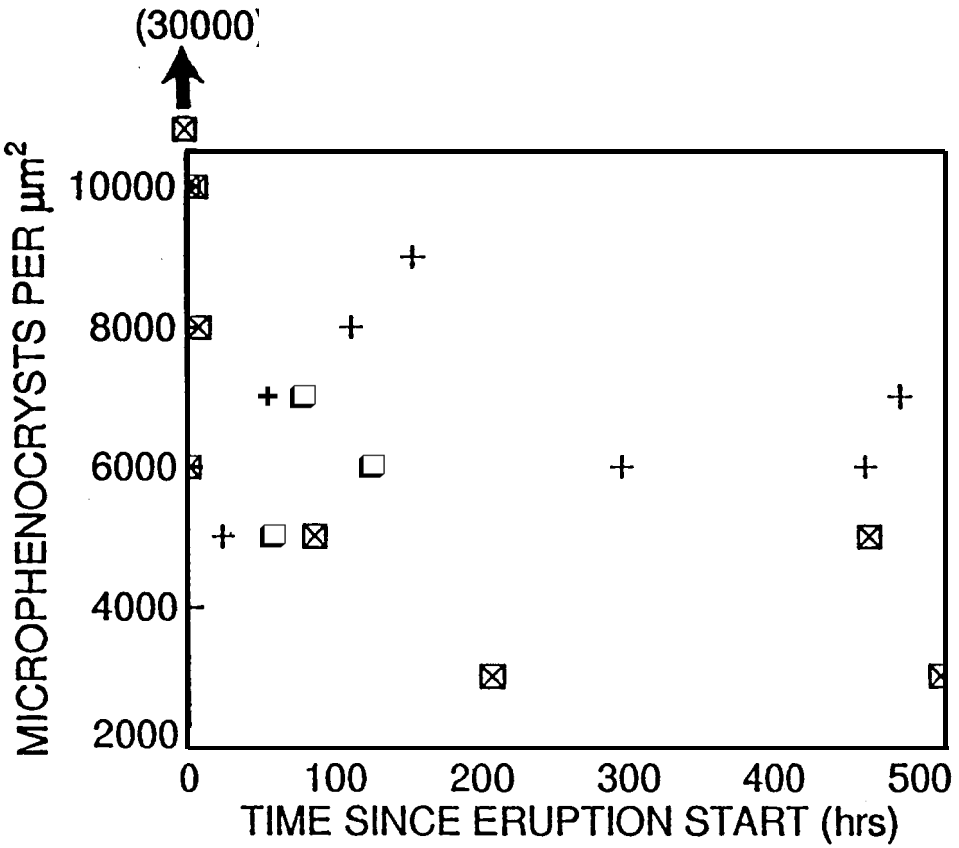
(30000)
MICROPHENOCRYSTS PER µm²
10000
8000
6000
4000
2000
0
100
200
300
400
500
TIME SINCE ERUPTION START (hrs)

Fig. 6

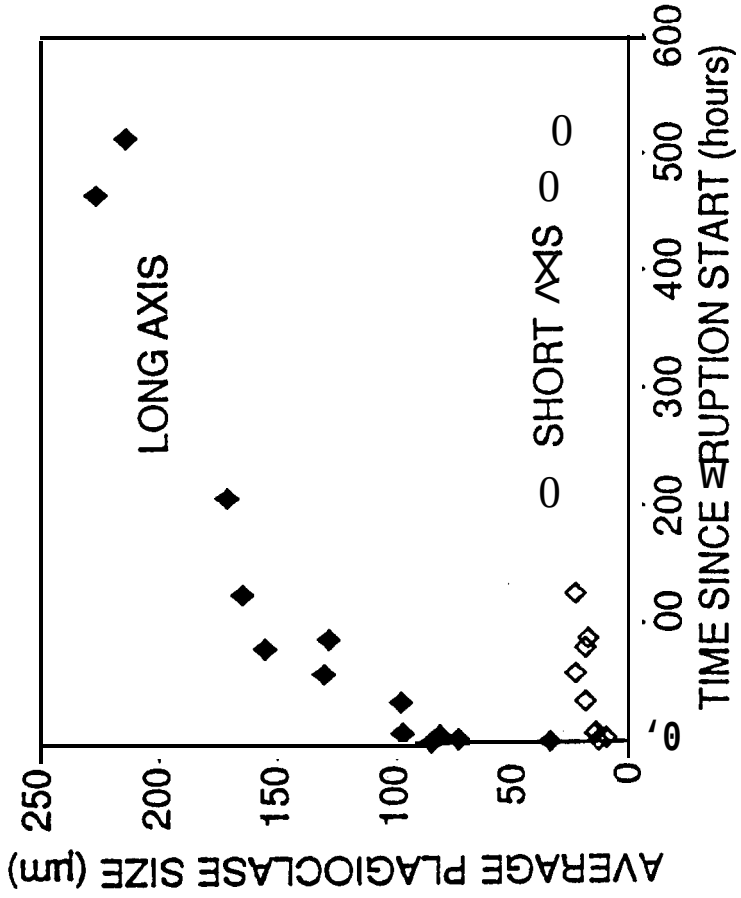
AVERAGE PLAGIOCLASE SIZE (μm)
250
200
150
100
50
0
0
200
300
400
500
600
TIME SINCE ERUPTION START (hours)
LONG AXIS
SHORT AXIS

Fig. 7

plagioclase long axis (Method A)
plagioclase short axis (A)
average microphenocryst size "m"
GROWTH RATE (cm s-1)
TIME SINCE ERUPTION START (hrs)
0
200
300
400
500

Fig. 8

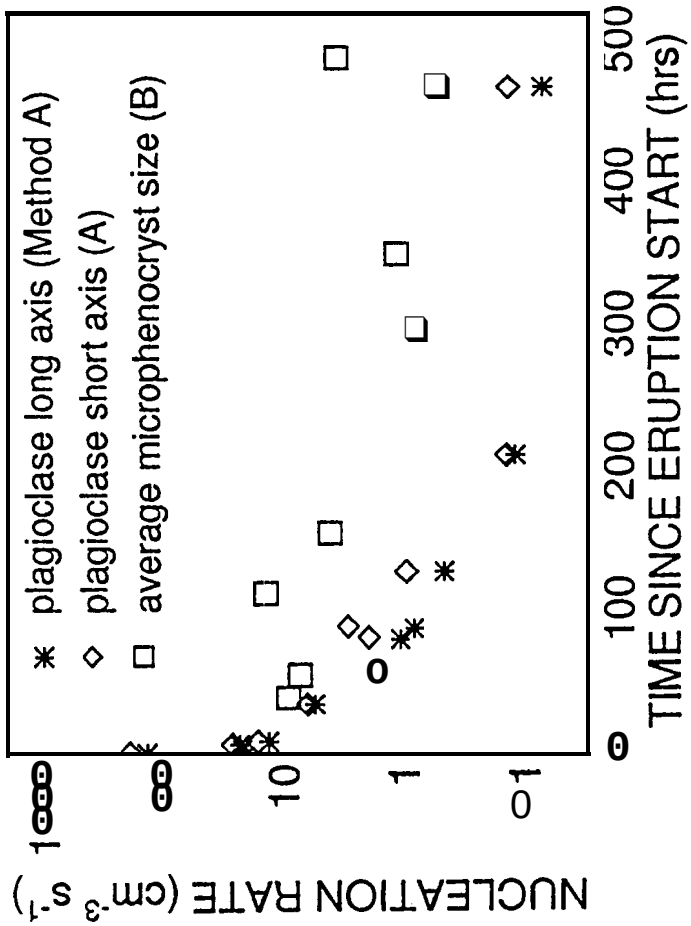
plagioclase long axis (Method A)
plagioclase short axis (A)
average microphenocryst size (B)
NUCLEATION RATE (cm-3 s-1)
TIME SINCE ERUPTION START (hrs)
0
100
200
300
400
500
10
1
0.1

Fig. ?

Fig. 10

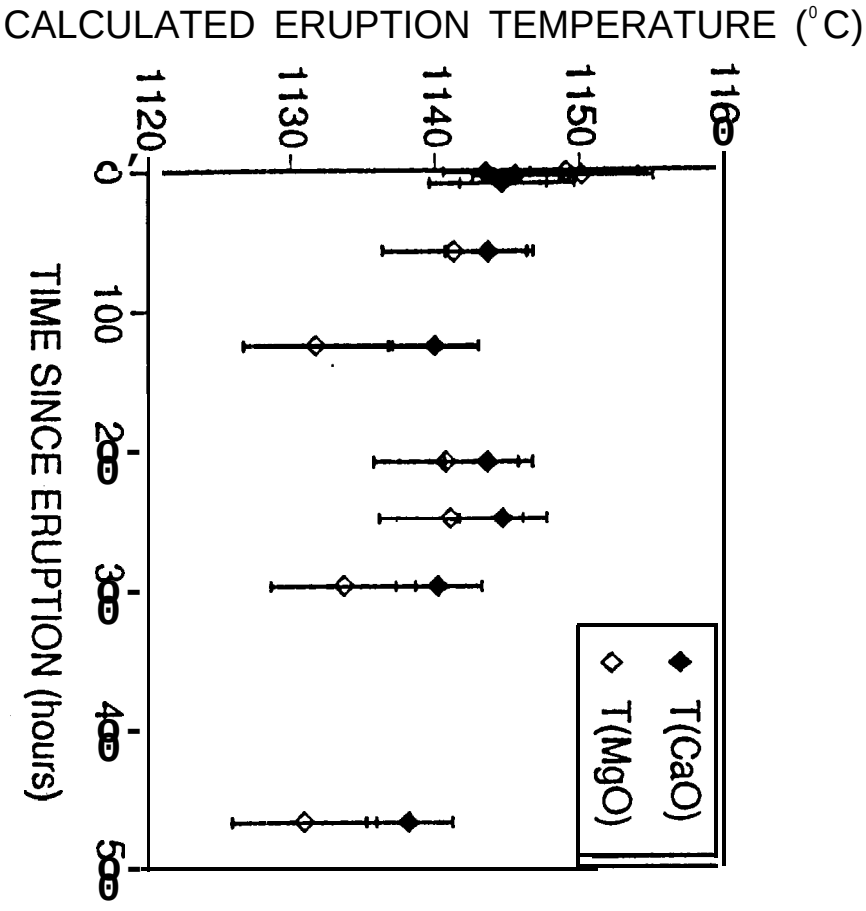
CALCULATED ERUPTION TEMPERATURE (°C)
1120
1130
1140
1150
1160
0
100
200
300
400
500
TIME SINCE ERUPTION (hours)
T(CaO)
T(MgO)

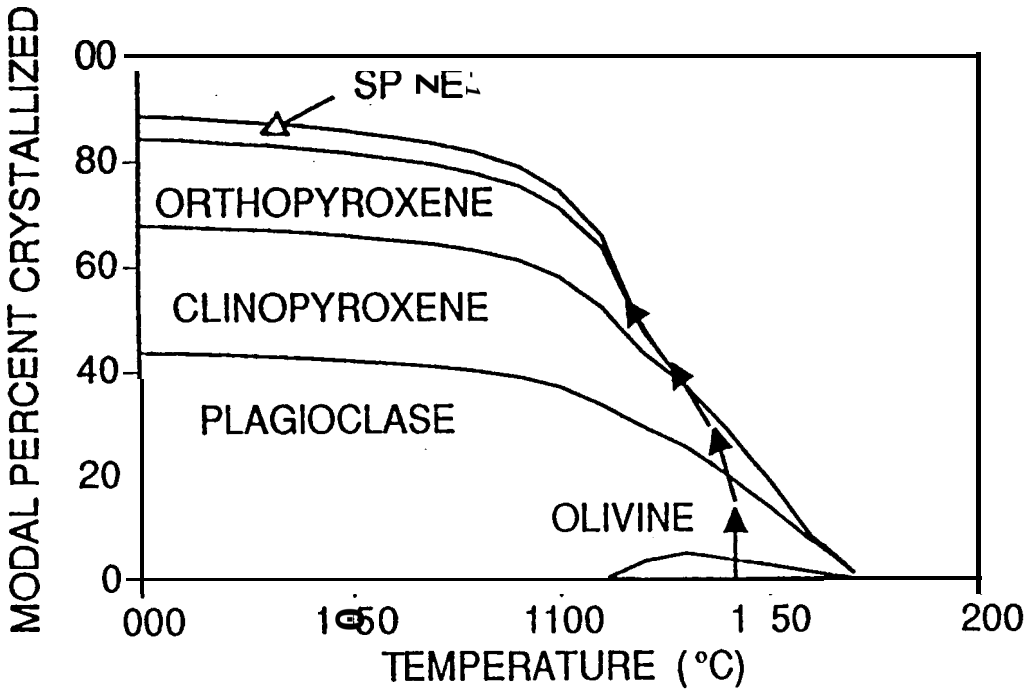
MODAL PERCENT CRYSTALLIZED
00
80
60
40
20
0
SP NE
ORTHOPYROXENE
CLINOPYROXENE
PLAGIOCLASE
OLIVINE
000
1100
1 50
200
TEMPERATURE (°C)

Fig. 11

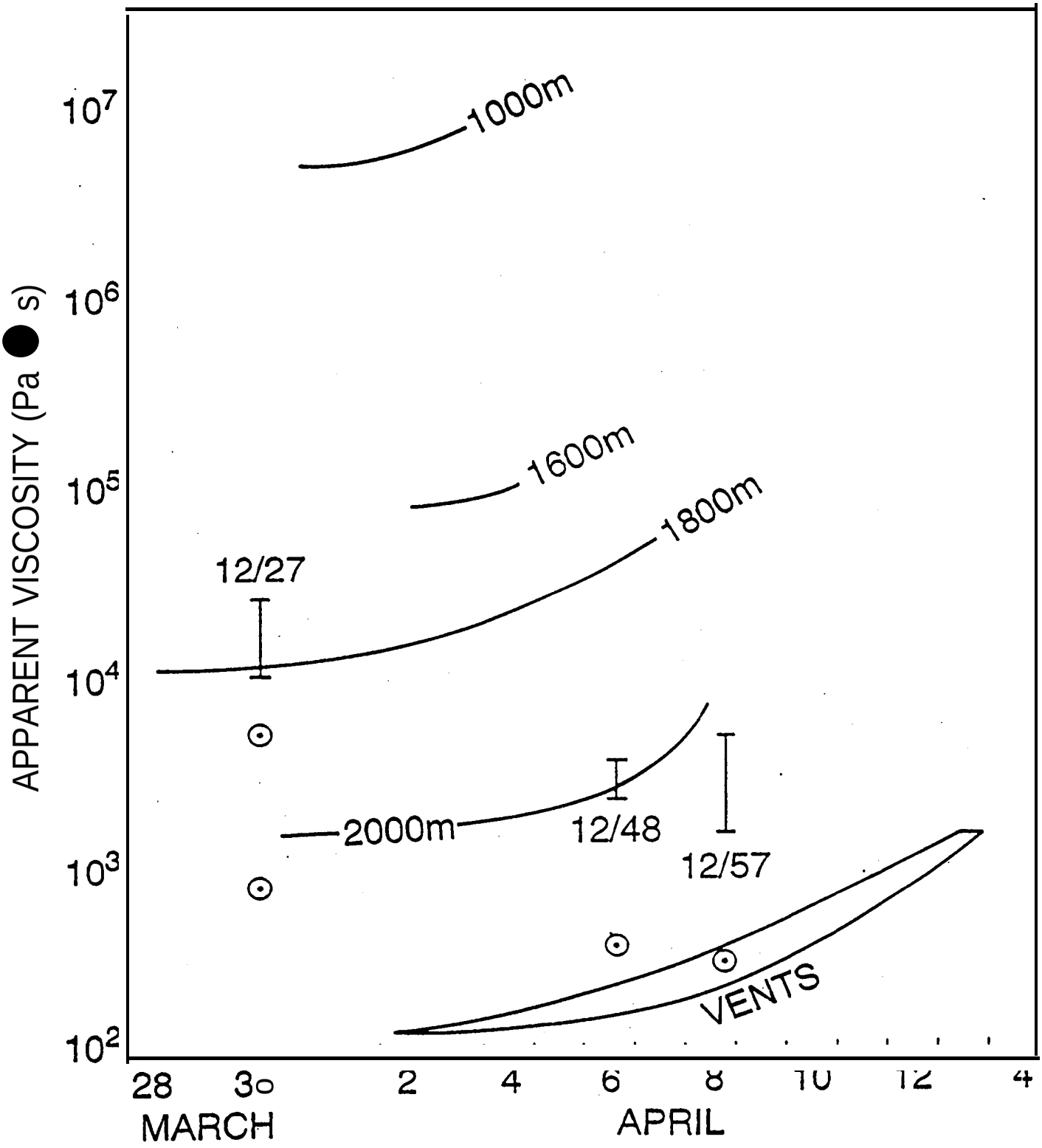
APPARENT VISCOSITY (Pa ● s)
10^7
10^6
10^5
10^4
10^3
10^2
1000m
1600m
1800m
2000m
12/27
12/48
12/57
VENTS
28
30
2
4
6
8
10
12
4
MARCH
APRIL

Fig. 12

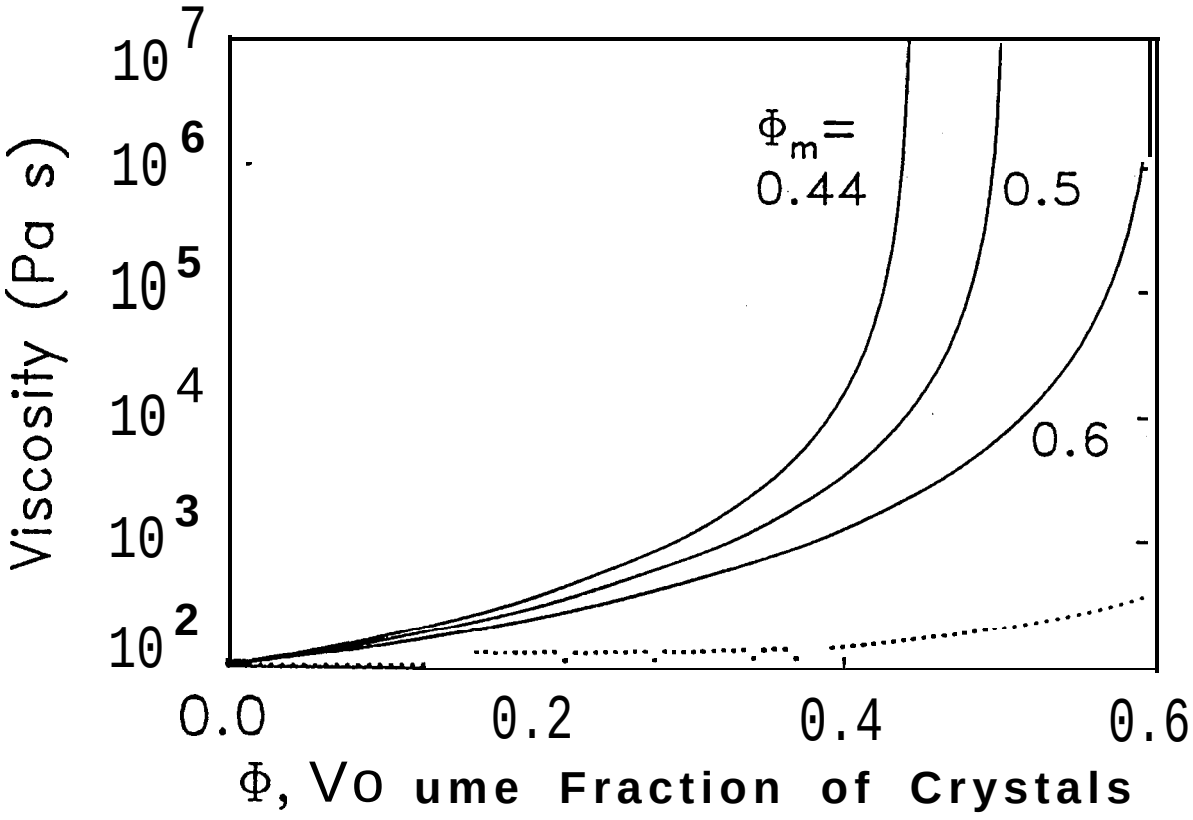
Viscosity (Pa s)
10^7
10^6
10^5
10^4
10^3
10^2
Φm=
0.44
0.5
0.6
0.0
0.2
0.4
0.6
Φ, Volume Fraction of Crystals

Fig. 13